AD-A169 096 A STUDY OF ENERGY CONVERSION DEVICES USING PHOTOACTIVE ORGANOMETALLIC ELE.. (U) MINNESOTA UNIV MINNEAPOLIS DEPT OF CHEMISTRY J F EVANS ET AL. 23 MAY 86 ARO-18767.9-CH 1/1

UNCLASSIFIED DAAG29-82-K-0063 F/G 10/2 NL

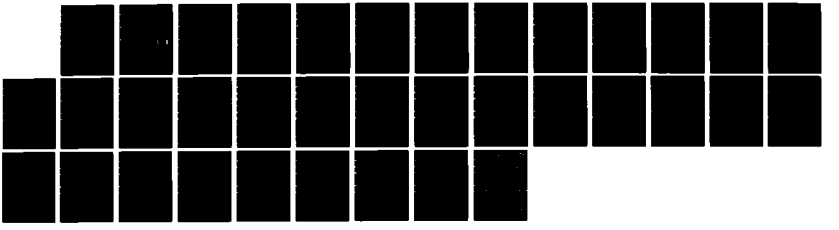

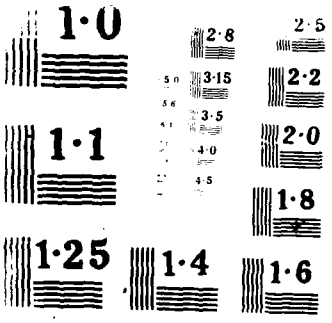
1·0
2·8
2·5
3·15
2·2
3·5
1·1
4·0
2·0
4·5
1·8
1·25
1·4
1·6

REPORT DOCUMENTATION PAGE

READ INSTRUCTIONS BEFORE COMPLETING FORM

1. REPORT NUMBER: ARO 18767.9-CH	2. GOVT ACCESSION NO.: N/A
3. RECIPIENT'S CATALOG NUMBER: N/A	
4. TITLE (and Subtitle): A Study of Energy Conversion Devices Using Photoactive Orgonometallic Electrocatalysts	5. TYPE OF REPORT & PERIOD COVERED: Final 2/82-6/85
	6. PERFORMING ORG. REPORT NUMBER:
7. AUTHOR(s): John F. Evans and Kent R. Mann	8. CONTRACT OR GRANT NUMBER(s): DAAG29-82-K-0063
9. PERFORMING ORGANIZATION NAME AND ADDRESS: Department of Chemistry, University of Minnesota, Minneapolis, MN 55455	10. PROGRAM ELEMENT, PROJECT, TASK AREA & WORK UNIT NUMBERS:
11. CONTROLLING OFFICE NAME AND ADDRESS: U. S. Army Research Office, Post Office Box 12211, Research Triangle Park, NC 27709	12. REPORT DATE: 23 May 1986
	13. NUMBER OF PAGES: 31
14. MONITORING AGENCY NAME & ADDRESS (if different from Controlling Office):	15. SECURITY CLASS. (of this report): Unclassified
	15a. DECLASSIFICATION/DOWNGRADING SCHEDULE:

16. DISTRIBUTION STATEMENT (of this report)

Approved for public release; distribution unlimited.

17. DISTRIBUTION STATEMENT (of the abstract entered in Block 20, if different from Report)

NA

18. SUPPLEMENTARY NOTES

The view, opinions, and/or findings contained in this report are those of the author(s) and should not be construed as an official Department of the Army position, policy, or decision, unless so designated by other documentation.

19. KEY WORDS (Continue on reverse side if necessary and identify by block number)

Photoelectrochemistry
Modified electrodes
Organometallics

20. ABSTRACT (Continue on reverse side if necessary and identify by block number)

Please See Reverse Side

DD FORM 1 JAN 73 1473 EDITION OF 1 NOV 65 IS OBSOLETE

ABSTRACT

The purpose of this project was to examine the feasibility of the use of transition metal hexakis arylisocyanide complexes confined to polymeric thin films in solar energy conversion systems. The chemical systems of interest were chromium, molybdenum and tungsten arylisocyanide complexes which had been previously examined in terms of their solution spectroscopy and photochemistry by Gray et al[1], and had been found to have rather long excited state lifetimes. Since we had shown that charge transfer complexes in thin polymer films supported on electrode surfaces were viable routes to solar energy conversion composites[2], we chose to extend our studies to include these more promising complexes.

The goals of the project then became threefold: 1) examine the thermodynamics and kinetics of charge transfer in the systems in which we had shown feasibility (polymeric ferrocenes) so as to understand the physical phenomena which were liable to control the overall efficiency and turnover numbers for the polymer bound photoelectrocatalysts, 2) further characterize the electrochemistry and physical inorganic chemistry of the more promising Cr, Mo and W hexakis arylisocyanide photoelectrocatalysts, and 3) examine ways by which these MLCT complexes could be entrapped in various polymer matrices. We have achieved success in the first two areas as described here. However, we were not succesful in finding a strategy by which these MLCT complexes could be reliably confined to a polymeric thin film supported on an inert electrode material while maintaining the electroactivity required to function as a photoelectochemical catalyst.

1. a) K.R. Mann, G.S. Hammond and H.B. Gray, J. Am. Chem. Soc., 99, 306 (1977); b) K.R. Mann, M. Cimolino, G.L. Geoffroy, G.S. Hammond, A.A. Orio, G. Albertini and H.B. Gray, Inorg. Chim. Acta, 16,97 (1976); c) K.R. Mann, Ph. D. Thesis, California Institute of Technology, Pasadena, CA, 1976.

2. a) M.F. Dautartas and J.F. Evans, J. Electroanal. Chem., 109 (1980) 301; b) M.F. Dautartas; K.R. Mann and J.F. Evans, Ibid., 110 (1980) 379.

A STUDY OF ENERGY CONVERSION DEVICES USING PHOTOACTIVE ORGANOMETALLIC ELECTROCATALYSTS

FINAL TECHNICAL REPORT

John F. Evans and Kent R. Mann

U.S. ARMY RESEARCH OFFICE

Contract Number: DAAG-29-82-K-0063

Department of Chemistry
University of Minnesota
Minneapois, MN 55455

TABLE OF CONTENTS

STATEMENT OF PROBLEM STUDIED

The purpose of this project was to examine the feasibility of the use of transition metal hexakis arylisocyanide complexes confined to polymeric thin films in solar energy conversion systems. The chemical systems of interest were chromium, molybdenum and tungsten arylisocyanide complexes which had been previously examined in terms of their solution spectroscopy and photochemistry by Gray et al[1], and had been found to have rather long excited state lifetimes.

Since we had shown that charge transfer complexes in thin polymer films supported on elkectrode surfaces were viable routes to solar energy conversion composites[2], we chose to extend our studies to include these more promising complexes. The goals of the project then became threefold: 1) examine the thermodynamics and kinetics of charge transfer in the systems in which we had shown feasibility (polymeric ferrocenes) so as to understand the physical phenomena which were liable to control the overall efficiency and turnover numbers for the polymer bound photoelectrocatalysts, 2) further characterize the electrochemistry and physical inorganic chemistry of the more promising Cr, Mo and W hexakis arylisocyanide photoelectrocatalysts, andf 3) examine ways by which these MLCT complexes could be entrapped in various polymer matrices. We have achieved success in the first two areas as described here. However, we were not succesful in finding a strategy by which these MLCT complexes could be reliably confined to a polymeric thin film supported on an inert electrode material while maintaining the electroactivity required to function as a photoelectochemical catalyst.

SUMMARY OF IMPORTANT RESULTS

We choose to summarize the results of the two succesful aspects of the project by reproducing the publications and portions of the manuscripts submitted for publication which resulted from this study. Because of difficulties in entrapping the ML_6 complexes in polymeric matrices, we wer not able, during this grant period, to examine the photoelectrochemistry of the targeted complexes

Reprinted from Inorganic Chemistry, 1983, 22, 1561

Contribution from the Department of Chemistry,
University of Minnesota, Minneapolis, Minnesota 55455

Synthesis, Characterization, and Properties of Stable Chromium(III) Aryl Isocyanide Complexes

David A. Bohling and Kent R. Mann*

Received August 9, 1982

The chemistry of homoleptic isocyanide complexes of chromium has been of interest[1-15] to organometallic chemists

(1) L. Malatesta, A. Sacco, and S. Ghielmi, *Gazz. Chim. Ital.*, **82**, 516 (1952)

since the synthesis of the zerovalent hexacoordinate aryl isocyanide derivatives by Malatesta[1,2] in the early 1950s. During the last 10 years, these compounds have been the subject to several electrochemical[7-10] and photochemical investigations,[11-14] showing that, although the Cr(0) complexes are formally isoelectronic with $Cr(CO)_6$, they possess strikingly different properties.[15] $Cr(CNAr)_6$, unlike $Cr(CO)_6$, can be sequentially oxidized in electrochemically reversible one-electron steps to produce the hexacoordinate Cr(I), Cr(II), and Cr(III) derivatives.[7] On the basis of these electrochemical results, Treichel et al.[8] isolated salts of the Cr(I) and Cr(II) derivatives by stoichiometrically oxidizing the zerovalent complexes with Ag^+ in acetone. However, the much more positive Cr(III)/Cr(II) formal potentials precluded the synthesis of the Cr(III) complexes by this route.[16] Complexes of the form $Cr(CNAr)_6^{3+}$ have been proposed as products in the disproportionation reaction (reaction 1) utilized in the synthesis of $Cr(CNAr)_6^0$, but no salts of the former have been isolated from this reaction.

$$3Cr_2(OAc)_4 \cdot 2H_2O + 36CNAr \rightarrow 2Cr(CNAr)_6^0 + 4Cr(CNAr)_6^{3+} + 12OAc^- + 6H_2O \quad (1)$$

While extending[17] the previous electrochemical studies, we became interested in isolating the Cr(III) derivatives to complete the series.[18] This unprecedented series affords the opportunity to systematically study the structure, bonding, and reactivity of complexes in which the metal attains four different oxidation states while maintaining identical ligation. By utilizing the powerful oxidants NO^+[19] and $SbCl_5$[20] at −25 °C, we have effected the synthesis and isolation of salts containing the $Cr(CNAr)_6^{3+}$ cations.

Experimental Section

Reagents. The synthesis of the starting materials $Cr(CNPh)_6$, $Cr(2,6\text{-}DMP)_6$, and $Cr(2,6\text{-}DiPP)_6$ have been previously reported.[17] $Cr(2,6\text{-}DMP)_6BF_4$ was prepared by the method of Treichel[8] substituting $AgBF_4$ for $AgPF_6$. $NOBF_4$ (Pfaltz and Bauer) and $SbCl_5$ (Aldrich) were used as received. Omnisolv methylene chloride and hexane were purchased from MCB and dried over activated alumina. AR grade anhydrous diethyl ether (Mallinckrodt) was protected from air and used as received.

Sample Handling. Because the solid Cr(III) products and their solutions are extremely mositure sensitive, they were handled by using either Schlenk techniques or a glovebag flushed with prepurified tank nitrogen. Nujol used for the infrared mull spectra was dried over $CaSO_4$. Even with extreme care, samples and solutions sometimes showed evidence of reaction with water. Many of the critical physical measurements were conducted on days of low absolute atmospheric humidity to enhance the effectiveness of the methods used to exclude moisture.

Physical Measurements. Infrared spectra were obtained as Nujol mulls on either a Beckman 4250 or a Perkin-Elmer 283. Elemental analyses were performed by Galbraith Laboratories, Knoxville, TN, and MHW Laboratories, Phoenix, AZ. The magnetic moment measurement was made on the solid material by the Faraday method.

Preparation of the Compounds. $Cr(2,6\text{-}DMP)_6(BF_4)_3$. A test tube with a total volume of about 60 mL was charged in a glovebag with 50.0 mg of $NOBF_4$ (0.43 mmol), 74.3 mg (0.08 mmol) of $Cr(2,6\text{-}DMP)_6BF_4$, and a stir bar, sealed with a serum stopper, and flushed with dry nitrogen. The tube was then placed in a low-temperature bath at −25 °C. Twenty milliliters of dry CH_2Cl_2 at −25 °C was transferred by cannula into the tube. The stirred solution underwent a series of color changes over 4 h, which terminated in a maroon solution. Fifty milliliters of cold, dry hexane was then added, precipitating a dark maroon microcrystalline solid. The mixture was filtered at −25 °C through a medium frit, yielding 76.5 mg of $Cr(2,6\text{-}DMP)_6(BF_4)_3$ (87% yield). Characteristic IR bands: $\bar{\nu}$(CN) 2214 cm^{-1} (s), $\bar{\nu}$(ring) 1588 cm^{-1} (m). Anal. Calcd for $C_{54}H_{54}N_6CrF_{12}B_3$: C, 58.99; H, 4.95; N, 7.64. Found: C, 58.95; H, 5.03; N, 7.45. Magnetic data: $\chi_M^{cor} = +6331 \times 10^{-6}$ cgsu/mol (diamagnetic correction -647×10^{-6} cgsu/mol), giving μ_{eff}(24 °C) = 3.89 μ_B.

$Cr(CNPh)_6(SbCl_6)_3$. A tube with a total volume of about 60 mL was charged with 105 mg of solid $Cr(CNPh)_6$ (0.15 mmol) and a stir bar and sealed. The tube was degassed with dry nitrogen by using flush/evacuate cycles and immersed in the −25 °C low-temperature bath. Twenty milliliters of dry CH_2Cl_2 was transferred by cannula into the tube through a glass stopcock equipped with a serum stopper. As the cold solution was stirred, 0.15 mL of $SbCl_5$ (1.2 mmol) was added by syringe. The solution immediately darkened and after several minutes deposited purple microcrystals. After an additional 4 h of stirring, the mixture was filtered through a medium frit. The solid product (250 mg, 95% yield) was washed with dry hexane. Characteristic IR bands: $\bar{\nu}$(CN) 2208 cm^{-1} (s), $\bar{\nu}$(ring) 1583 cm^{-1} (s). Anal. Calcd for $C_{42}H_{30}N_6CrCl_{18}Sb_3$: C, 30.13; H, 1.81; N, 5.02. Found: C, 29.92; H, 2.09; N, 5.00.

$Cr(2,6\text{-}DMP)_6(SbCl_6)_3$. A method virtually identical with that used for the phenyl isocyanide complex was used for this case, with the exception that the product, which was partially soluble in cold CH_2Cl_2, was precipitated as dark purple microcrystals on addition of 30 mL of cold, dry hexane. One hundred milligrams of $Cr(2,6\text{-}DMP)_6$ (0.12 mmol) yielded 164 mg of $Cr(2,6\text{-}DMP)_6(SbCl_6)_3$ (75%). Characteristic IR bands: $\bar{\nu}$(CN) 2188 cm^{-1} (s), $\bar{\nu}$(ring) 1587 cm^{-1} (s). Anal. Calcd for $C_{54}H_{54}N_6CrCl_{18}Sb_3$: C, 35.20; H, 2.95; N, 4.56; Cl, 34.64. Found: C, 35.03; H, 3.03; N, 4.46; Cl, 34.38.

$Cr(2,6\text{-}DiPP)_6(SbCl_6)_3$. The method used was the same as for the 2,6-DMP compound. One hundred milligrams of $Cr(2,6\text{-}DiPP)_6$ (0.085 mmol) yielded 148 mg of blue microcrystalline $Cr(2,6\text{-}DiPP)_6(SbCl_6)_3$ (80% yield). Characteristic IR bands: $\bar{\nu}$(CN) 2180 cm^{-1} (vs), $\bar{\nu}$(ring) 1585 (s). Anal. Calcd for $C_{78}H_{102}N_6CrCl_{18}Sb_3$: C, 42.99; H, 4.72; N, 3.86. Found: C, 42.74; H, 4.79; N, 3.81.

$Cr(2,6\text{-}DMP)_6(BF_4)_2 \cdot 8H_2O \cdot HBF_4$. A solid sample (~20 mg) of $Cr(2,6\text{-}DMP)_6(BF_4)_3$ exposed to air for 4 days yielded an orange powder. IR spectrum: $\bar{\nu}$(CN) 2147 cm^{-1} (vs), $\bar{\nu}$(ring) 1588 cm^{-1} (m). Anal. Calcd for $C_{54}H_{71}N_6O_8CrF_{12}B_3$: C, 52.11; H, 5.75; N, 6.75. Found: C, 52.40; H, 5.44; N, 6.74.

Discussion

Treatment of $Cr(2,6\text{-}DMP)_6^+$ or $Cr(2,6\text{-}DMP)_6$ (2,6-DMP = 2,6-dimethylphenyl isocyanide) with an excess of either $NOBF_4$ or $SbCl_5$ in dry CH_2Cl_2 at −25 °C results in a rapid sequence of color changes terminating in a dark solution, which on standing at −25 °C deposits microcrystals of the maroon BF_4^- or purple $SbCl_6^-$ salts of the $Cr(2,6\text{-}DMP)_6^{3+}$ cation. Filtration of the solution under dry nitrogen affords ~85% yield of the microcrystalline compounds which are stable at room temperature in the absence of water. The infrared

(2) L. Malatesta and A. Sacco, *Atti Accad. Naz. Linci, Cl. Sci. Fis., Mat. Nat., Rend.* [8] **13**, 264 (1952).
(3) F. A. Cotton and F. Zingales, *J. Am. Chem. Soc.*, **83**, 351 (1961).
(4) K. R. Mann, M. Cimolino, C. L. Geoffroy, G. S. Hammond, A. A. Orio, G. Albertin, and H. B. Gray, *Inorg. Chim. Acta*, **16**, 97 (1976).
(5) K. R. Mann, Ph.D. Thesis, California Institute of Technology, 1976.
(6) Evert Ljungström, *Acta Chem. Scand., Ser. A*, **A32**, 47 (1978).
(7) P. M. Treichel and G. J. Essenmacher, *Inorg. Chem.*, **15**, 146 (1976).
(8) G. J. Essenmacher and P. M. Treichel, *Inorg. Chem.*, **16**, 800 (1977).
(9) P. M. Treichel, D. W. Firsich, and G. J. Essenmacher, *Inorg. Chem.*, **18**, 2405 (1979).
(10) W. S. Mialki, T. E. Wood, and R. A. Walton, *J. Am. Chem. Soc.*, **102**, 7105 (1980).
(11) K. Iuchi, S. Asada, and A. Sugimori, *Chem. Lett.*, 801 (1974).
(12) K. Iuchi, S. Asada, T. Kinugasa, K. Kanamori, and A. Sugimori, *Bull. Chem. Soc. Jpn.*, **49**, 577 (1976).
(13) K. R. Mann, G. S. Hammond, and H. B. Gray, *J. Am. Chem. Soc.*, **99**, 306 (1977).
(14) H. B. Gray, K. R. Mann, N. S. Lewis, J. A. Thich, and R. M. Richman, *Adv. Chem. Ser.*, **No. 168**, 44 (1978).
(15) F. A. Cotton and G. Wilkinson, "Advanced Inorganic Chemistry", 4th ed., Wiley, New York, 1980, pp 93–95.
(16) The electrochemical syntheses of $Cr(CNR)_6^{3+}$ complexes, where R = alkyl, have been unsuccessfully attempted: W. S. Mialki, D. E. Wigley, T. E. Wood, and R. A. Walton, *Inorg. Chem.*, **21**, 480 (1982).
(17) D. A. Bohling, J. F. Evans, and K. R. Mann, *Inorg. Chem.*, **21**, 3546 (1982).
(18) These complexes are isoelectronic with vanadium(II) alkyl isocyanide complexes that have been recently characterized by: I. D. Silverman, J. C. Dewan, C. M. Giandomenico, and S. J. Lippard, *Inorg. Chem.*, **19**, 3379 (1980); I. D. Silverman, P. W. R. Corfield, and S. J. Lippard, *ibid.*, **20**, 3106 (1981).
(19) N. G. Connelly and J. D. Davies, *J. Organomet. Chem.*, **38**, 385 (1972).
(20) $SbCl_5$ has been used in chlorinated organic solvents to produce powerfully oxidizing organic cation radicals: E. A. Bell, A. Ledwith, and D. C. Sherrington, *J. Chem. Soc. C*, 2719 (1969).

spectra of these two compounds exhibit single, very strong $\bar{\nu}$(CN) stretches at 2214 and 2188 cm^{-1}, respectively. The elemental analyses that were obtained for these compounds are in excellent agreement with their formulation as $Cr(2,6\text{-}DMP)_6(BF_4)_3$ and $Cr(2,6\text{-}DMP)_6(SbCl_6)_3$. Measurement of the magnetic susceptibility at 24 °C of the BF_4^- salt gave a value of 3.89 μ_B for the magnetic moment, consistent with the spin-only value expected for three unpaired electrons residing on a pseudooctahedral Cr(III) center.

Similar reactions were carried out on the unsubstituted parent compound, $Cr(CNPh)_6$, using $NOBF_4$, $NOPF_6$, or $SbCl_5$ as the oxidant. Solid compounds were isolated in each case, which exhibited $\bar{\nu}$(CN) stretching frequencies at about 2210 cm^{-1}. However, only in the case of $SbCl_5$ was an analytically pure compound obtained. $Cr(CNPh)_6(SbCl_6)_3$ is a deep purple microcrystalline solid, which exhibits an intense $\bar{\nu}$(CN) stretching frequency at 2208 cm^{-1}, indicative of an extremely electron-deficient environment at the Cr(III) center.[21]

The isolation and thermal stability of these chromium(III) isocyanide derivatives are surprising in view of their highly oxidizing nature. While the formal reduction potentials for the CrL_6^{3+}/CrL_6^{2+} couples are quite positive for L = phenyl isocyanide and 2,6-DMP (+0.73 and +0.82 V, respectively, vs. corrected AgCl/Ag in CH_2Cl_2 with 0.1 M TBAH as the electrolyte),[17] the isolation of $Cr(2,6\text{-}DiPP)_6(SbCl_6)_3$ (2,6-DiPP = 2,6-diisopropylphenyl isocyanide), with a formal Cr(III)/Cr(II) reduction potential of +1.27 V vs. AgCl/Ag, is particularly amazing. This latter compound was obtained as a blue microcrystalline solid, which is stable in the absence of water, as are the other Cr(III) complexes described here.

The oxidizing nature of these compounds is illustrated by their solid-state reactivity. Remarkably, in solid $Cr(2,6\text{-}DMP)_6(BF_4)_3$, the $Cr(2,6\text{-}DMP)_6^{3+}$ cation is *cleanly* reduced to $Cr(2,6\text{-}DMP)_6^{2+}$ simply by exposing the solid to the atmosphere for several days. The color of the solid sample lightens from the maroon color of the Cr(III) complex to the orange color characteristic of the corresponding Cr(II) complex. The analysis of the resulting solid agrees closely with the formulation $Cr(2,6\text{-}DMP)_6(BF_4)_2 \cdot 8H_2O \cdot HBF_4$, and the compound exhibits an intense $\bar{\nu}$(CN) stretch in the infrared spectrum at 2147 cm^{-1}. Upon further, prolonged exposure to air, this solid becomes light green, with the $\bar{\nu}$(CN) band at 2147 cm^{-1} disappearing, as a new band at 1650 cm^{-1} indicative of isocyanide ligand hydrolysis grows in. At this time, we can only speculate that the reducing atmospheric component in this system is water, which reduces the Cr(III) complex to the Cr(II) complex. The less sterically hindered $Cr(CNPh)_6^{3+}$ cation appears decidedly more reactive with the atmosphere, bypassing completely the reduction stage, proceeding directly to the ligand hydrolysis stage after only a few hours. We intend to investigate these solid-state transformations more completely in the future.

Perhaps the most interesting chemistry these Cr(III) complexes exhibit is the extreme lability of the isocyanide ligands in room-temperature solutions, confirming observations made in cyclic voltammetric measurements on $Cr(2,6\text{-}DMP)_6^{3+}$ and $Cr(2,6\text{-}DiPP)_6^{3+}$.[17] While "typical" Cr(III) complexes undergo ligand exchange with first-order rate constants on the order of 10^{-6} s^{-1} ($Cr(H_2O)_6^{3+}$), room-temperature dissolution of the $Cr(CNAr)_6^{3+}$ complexes in acetone, acetonitrile, or propylene carbonate leads to instantaneous bleaching. These solutions show strong bands in the infrared region near 2120 cm^{-1}, characteristic of the $\bar{\nu}$(CN) stretching frequency of uncoordinated aryl isocyanides. These apparently facile ligand replacement reactions can also be contrasted to the behavior of the zerovalent low-spin d^6 $Cr(CNPh)_6$ complex, which exhibits a first-order ligand-exchange rate constant of 2.8×10^{-7} s^{-1} at 20 °C.[22]

In view of these facile ligand replacement reactions, the apparent ease of hydrolysis in the solid state, and the strongly oxidizing nature of these Cr(III) complexes, we conclude that the further development of their chemistry will yield quite interesting results.

Acknowledgment. This work was supported by the U.S. Army Research Office.

Registry No. $Cr(2,6\text{-}DMP)_6(BF_4)_3$, 85135-14-4; $Cr(CNPh)_6(SbCl_6)_3$, 85150-70-5; $Cr(2,6\text{-}DMP)_6(SbCl_6)_3$, 85135-15-5; $Cr(2,6\text{-}DiPP)_6(SbCl_6)_3$, 85135-16-6; $Cr(2,6\text{-}DMP)_6(BF_4)_2$, 85135-17-7; $Cr(2,6\text{-}DMP)_6BF_4$, 85135-18-8; $Cr(CNPh)_6$, 17375-15-4; $Cr(2,6\text{-}DMF)_6$, 82456-65-3; $Cr(2,6\text{-}DiPP)_6$, 82456-71-1.

(21) There is a correlation between the Cr oxidation state in $Cr(CNAr)_6^{n+}$ compounds and the $\bar{\nu}$(CN) stretching frequency. For example, for Ar = Ph: $n = 0$, $\bar{\nu}$(CN) 1975 cm^{-1}; $n = 1$, $\bar{\nu}$(CN) 2065 cm^{-1}; $n = 2$, $\bar{\nu}$(CN) 2161 cm^{-1} (data from ref 7).

(22) G. Cetini and O. Gambino, *Ann. Chim. (Rome)*, **53**, 236 (1963).

Reprinted from Inorganic Chemistry, 1984, 23, 1126

Contribution from the Department of Chemistry,
University of Minnesota, Minneapolis, Minnesota 55455

X-ray Structural Characterization of $[Cr(CNPh)_6][CF_3SO_3]$, $[Cr(CNPh)_6][PF_6]_2$, and $[Cr(CNPh)_6][SbCl_6]_3 \cdot CH_2Cl_2$. Completion of a Unique Series of Complexes in Which the Metal Attains Four Different Oxidation States While Maintaining Identical Ligation

DAVID A. BOHLING and KENT R. MANN*

Received June 14, 1983

The crystal structures of $[Cr(CNC_6H_5)_6][CF_3SO_3]$ (A), $[Cr(CNC_6H_5)][PF_6]_2$ (B), and $[Cr(CNC_6H_5)_6][SbCl_6]_3 \cdot CH_2Cl_2$ (C) have been determined by single-crystal X-ray diffraction techniques. Compound A crystallizes in the $P2_1/n$ (No. 14) space group with $Z = 2$, $V = 2061$ (2) Å^3, $a = 10.757$ (3) Å, $b = 19.994$ (6) Å, $c = 10.242$ (3) Å, and $\beta = 110.69$ (20)°. Full-matrix least-squares refinement (264 variables, 3679 reflections) converged to give R and R_w values of 0.042 and 0.061, respectively. The structure of A consists of discrete $[Cr(CNC_6H_5)_6]^+$ cations and disordered $[CF_3SO_3]^-$ anions. A minor Jahn–Teller distortion is observed in the Cr–C bond lengths, which average 1.975 Å. Compound B crystallizes in the $P2_1/n$ (No. 14) space group with $Z = 4$, $V = 4365$ (5) Å^3, $a = 13.888$ (4) Å, $b = 19.638$ (4) Å, $c = 16.009$ (11) Å, and $\beta = 91.20$ (4)°. Least-squares refinement (329 variables, 2335 reflections) gave $R = 0.060$ and $R_w = 0.070$. The Cr site is a general position in the unit cell. The ligands show a pronounced C_{2v} angular distortion with the C–Cr–C bond angles ranging from 83.7 to 97.0°. The Cr–C bonds average 2.014 Å. Compound C crystallizes in the *Cccm* (No. 66) space group with $Z = 4$, $V = 6483$ (6) Å^3, $a = 14.818$ (6) Å, $b = 18.450$ (5) Å, $c = 23.714$ (7) Å, and $\beta = 90.0$°. Full-matrix least-squares refinement (180 variables, 1445 reflections) converged to give $R = 0.058$ and $R_w = 0.059$. The CH_2Cl_2 of crystallization was disordered. The four crystallographically related equatorial ligands exhibit Cr–C bonds of 2.049 (10) Å relative to the long Cr–C axial bonds of 2.091 (14) Å. Changes in the Cr–C and C≡N bond lengths are discussed in relation to the d-electron configuration of the central metal. The origin of the large positive value previously obtained for the $Cr(CNPh)_6^{3+}/Cr(CNPh)_6^{2+}$ reduction potential is discussed in relation to the large negative value reported for the $Cr(CN)_6^{3-}/Cr(CN)_6^{4-}$ couple.

Introduction

Recently, we have extended[1] previous investigations[2] of the electrochemical behavior of ring-substituted, six-coordinate aryl isocyanide complexes of Cr(0), Cr(I), Cr(II), and Cr(III). During the course of this work, we developed high-yield syntheses for the previously unavailable, highly reactive Cr(III) complexes.[3] We became interested in broadening our research effort in this area because the $Cr(CNAr)_6^{n+}$ series offers an opportunity unique in organometallic transition-metal chemistry: structure, bonding, and reactivity studies are feasible on compounds in which the metal center retains identical ligation in four different oxidation states.[4]

As an important part of these studies, we set out to complete the structural characterization of the $Cr(CNPh)_6^{n+}$ ($n = 0$–3) series by X-ray diffraction techniques. Of these four complexes, only the structure of $Cr(CNPh)_6$ had been previously determined.[5] Herein we report the X-ray crystal structure determinations of $[Cr(CNPh)_6][CF_3SO_3]$, $[Cr(CNPh)_6][PF_6]_2$, and $[Cr(CNPh)_6][SbCl_6]_3 \cdot CH_2Cl_2$.

Experimental Section

General Considerations. Omnisolv dichloromethane and hexane were purchased from MCB and dried over activated alumina. $AgCF_3SO_3$ and $AgPF_6$ were purchased from Alfa Products. $Cr(CNPh)_6$ was synthesized by the method of Malatesta.[6] $[Cr(CNPh)_6][CF_3SO_3]$ and $[Cr(CNPh)_6][PF_6]_2$ were prepared by the method of Treichel[2b] ($AgCF_3SO_3$ was substituted for $AgPF_6$ in the first case).

Suitable crystals of $[Cr(CNPh)_6][CF_3SO_3]$ (yellow-brown) and $[Cr(CNPh)_6][PF_6]_2$ (yellow) for X-ray crystallographic studies were grown by allowing hexane to slowly diffuse with dichloromethane solutions of the compounds at 0 °C over a period of several days.

The crystal of $[Cr(CNPh)_6][SbCl_6]_3 \cdot CH_2Cl_2$ (red) used in this study was grown by carefully layering −20 °C solutions of $Cr(CNPh)_6^0$ (top) and $SbCl_5$ in dry CH_2Cl_2 in a Schlenk tube. Crystals of $[Cr(CNPh)_6][SbCl_6]_3 \cdot CH_2Cl_2$ grew at the solution interface over a period of 3 weeks. Attempts to grow crystals of several other salts (PF_6^-, SbF_6^-, AsF_6^-) of the $Cr(CNPh)_6^{3+}$ cation were unsuccessful.[7]

Crystal Handling. Crystals of $[Cr(CNPh)_6][CF_3SO_3]$ and $[Cr(CNPh)_6][PF_6]_2$ were mounted on standard glass fibers with use of an epoxy resin. Neither of these compounds in the solid state showed sensitivity to water or air when exposed to normal laboratory conditions.

The Cr(III) compound is extremely reactive toward atmospheric water and uncured epoxy resins. The crystal of $[Cr(CNPh)_6][SbCl_6]_3 \cdot CH_2Cl_2$ was suspended in dry Nujol and then wedged into a glass capillary tube; the capillary was then sealed at both ends with epoxy. Crystals mounted in this way were found to be stable over the data collection period.

Summaries of the crystal data and collection parameters for the three compounds are found in Table I.

Structure Solutions General Remarks. The automatic peak searching, centering, and indexing routines available on the Enraf-Nonius SDP-CAD4 automatic diffractometer[7] were used to find and center 25 reflections, which were used to determine the unit cell parameters. Space group assignments were made by examining the data collected for systematic absences and confirmed by the successful solution and refinement of the structures. Data processing and reduction,[7] Patterson function, Fourier and difference Fourier syntheses,

(1) Bohling, D. A.; Evans, J. F.; Mann, K. R. *Inorg. Chem.* **1982**, *21*, 3546.
(2) (a) Treichel, P. M.; Dirreen, G. E. *J. Organomet. Chem.* **1972**, *39*, C20. (b) Treichel, P. M.; Essenmacher, G. J. *Inorg. Chem.* **1976**, *15*, 146. (c) Essenmacher, G. J.; Treichel, P. M. *Ibid.* **1977**, *16*, 800. (d) Treichel, P. M.; Firsich, D. W.; Essenmacher, G. J. *Ibid.* **1979**, *18*, 2405.
(3) Bohling, D. A.; Mann, K. R. *Inorg. Chem.* **1983**, *22*, 1561.
(4) "Redox chains" have been reported previously for coordination compounds. For example, see: Vlček, A. A. *Nature (London)* **1961**, *189*, 393. Baker, B. R.; Mehta, B. D. *Inorg. Chem.* **1965**, *4*, 848. Hughes, M. C.; Macero, D. J. *Ibid.* **1976**, *15*, 2040. Tanaka, N.; Sato, Y. *Inorg. Nucl. Chem. Lett.* **1968**, *4*, 457. Tanaka, N.; Sato, Y. *Bull. Chem. Soc. Jpn.* **1969**, *42*, 1021. Pierpont, C. G.; Buchanan, R. M. *Inorg. Chem.* **1982**, *21*, 652.
(5) (a) Ljungstrom, E. *Acta Chem. Scand., Ser. A* **1978**, *32*, 47. (b) Mann, K. R. Ph.D. Thesis, California Institute of Technology, 1976. (c) Gray, H. B.; Mann, K. R.; Lewis, N. S.; Thich, J. A.; Richman, R. M. *Adv. Chem. Ser.* **1978**, *No. 168*, 44.
(6) Malatesta, L.; Sacco, A.; Gheimi, S. *Gazz. Chim. Ital.* **1952**, *82*, 516. Malatesta, L.; Sacco, A. *Atti Accad. Naz. Lincei, Cl. Sci. Fis., Mat. Nat., Rend.* **1952**, *13*, 264.
(7) Bohling, D. A.; Mann, K. R.; unpublished results.
(8) All calculations were carried out on PDP 8/A and 11/34 computers using the Enraf-Nonius CAD4-SDP programs. This crystallographic computing package is described in: Frenz, B. A. In "Computing in Crystallography"; Schenk, H., Olthof-Hazekamp, R., van Koningsveld, H., Bassi, G. C., Eds.; Delft University Press: Delft, Holland, 1978; pp 64–71. "CAD4 SDP Users Manual"; Enraf-Nonius: Delft, Holland, 1979.

Table I. Crystal Data and Collection Parameters

	Cr(I)	Cr(II)	Cr(III)
compd	$[Cr(CNPh)_6][CF_3SO_3]$	$[Cr(CNPh)_6][PF_6]_2$	$[Cr(CNPh)_6][SbCl_6]_2 \cdot CH_2Cl_2$
formula	$C_{43}H_{30}N_6F_3O_3SCr$	$C_{42}H_{30}N_6F_{12}P_2Cr$	$C_{51}H_{32}N_6Cl_{20}Sb_2Cr$
fw	819.81	960.67	1759.12
space group	$P2_1/n$ (No. 14)	$P2_1/n$ (No. 14)	$Ccem$ (No. 66)
a, Å	10.757 (3)	13.888 (4)	14.818 (6)
b, Å	19.994 (6)	19.638 (4)	18.450 (5)
c, Å	10.242 (3)	16.009 (11)	23.714 (7)
β, deg	110.69 (20)	91.20 (4)	90.00
V, Å^3	2061 (2)	4365 (5)	6483 (6)
Z	2	4	4
d(calcd), g cm^{-3}	1.321 (1)	1.452 (2)	1.802 (2)
d(obsd), g cm^{-3}	1.314 (5)	1.423 (5)	1.746 (5)
cryst size, mm	0.26 × 0.26 × 0.31	0.08 × 0.10 × 0.31	0.16 × 0.31 × 0.36
μ, cm^{-1}	33.6	37.7	22.7
radiation (graphite monochromated)	Cu (λ = 1.541 84 Å)	Cu (λ = 1.541 84 Å)	Mo (λ = 0.710 73 Å)
scan type	ω–2θ	ω–2θ	ω–2θ
collection range, deg	2θ = 0–156	2θ = 0–96	2θ = 0–50
no. of unique data	4735	4493	3149
no. of data for $F^2 > \sigma(F^2)$	3679	2335	1445
P	0.05	0.05	0.04
no. of variables	264	329	180
R	0.042	0.060	0.058
R_w	0.061	0.070	0.059

and least-squares refinement[10] were carried out with use of the computer programs available in the Enraf-Nonius structure-solving package. Scattering factors were from Cromer and Waber[11] and included the effects of anomalous dispersion.[12]

$[Cr(CNPh)_6][SO_3CF_3]$. Over the course of data collection, the check reflections showed a maximum decrease of 7%. The data were corrected for this decomposition. No absorption corrections were made. A total of 4735 independent reflections were collected by the ω–2θ scan technique in the scan range 2θ = 0–156°. Space group $P2_1/n$ (No. 14) was indicated by the systematic absences in the data, which were collected in the hkl and $h\bar{k}l$ octants. The trial solution, which placed the Cr atom at the origin, yielded R = 0.55 and allowed 11 more atoms to be placed by examination of the differences Fourier. Sequences of least-squares refinement, Fourier, and difference Fourier allowed the placement of all the non-hydrogen atoms. Full-matrix least-squares refinement (264 variables) utilizing anisotropic temperature factors for all non-hydrogen atoms and idealized placement of the H atoms with temperature factors (B) fixed at 8.0 Å^2 converged to give R and R_w values of 0.042 and 0.061, respectively. The error in an observation of unit weight was 1.742, based on a value of 0.05 for p in the $\sigma(I)$ equation.[9]

Disorder was found in the $CF_3SO_3^-$ counterion.[13] The nature of the disorder is based on the approximate equality of the SO_3 and CF_3 halves of the ion. The conformation of $CF_3SO_3^-$ is staggered so that the CF_3 and SO_3 groups are randomly disordered about the pseudo inversion center. The apparent C and S atoms were modeled with the assumption of half-occupied anisotropic S and a half-occupied C with a fixed isotroic temperature factor (B) of 10.0 Å^2. The apparent F and O sites were similarly modeled, but with a fully occupied anisotropic O–F average atom. The model for the disorder was judged adequate by the absence of any significant electron density peaks in the final difference Fourier in this region of the unit cell.

$[Cr(CNPh)_6][PF_6]_2$. During data collection no decrease or fluctuations were observed in the check reflections. A total of 4493 independent reflections were collected by the ω–2θ scan technique in the rather limited range 2θ = 0–96°. High-angle scattering (2θ > 96°) was poor, perhaps because of the small crystal size. Larger crystals were unavailable. Absorption corrections were not made. The space group $P2_1/n$ (No. 14) was indicated by the systematic absences in the data, which were collected in octants hkl and $h\bar{k}l$. Examination of the Patterson function led to no physically reasonable solution of the structure; direct methods were then employed. The program MULTAN[14] was used to generate an electron density map, which allowed the placement of the Cr atom, 1 of the 2 P atoms, and 41 of the light atoms into chemically reasonable positions.

Sequences of least-squares refinement and Fourier and difference Fourier allowed the placement of all non-hydrogen atoms. Full-matrix least-squares refinement (329 variables), which utilized anisotropic temperature factors for Cr, P, and F, isotropic temperature factors for C and N, and idealized placement of the H atoms with temperature factors (B) fixed at 6.0 Å^2, converged to give R = 0.06 and R_w = 0.070. The error in an observation of unit weight was 1.954, based on a value of 0.05 for the p in the $\sigma(I)$ equation.[9]

$[Cr(CNPh)_6][SbCl_6]_2 \cdot CH_2Cl_2$. During data collection no decrease or fluctuations were observed in the check reflections. A total of 3149 independent reflections were collected by the ω–2θ scan technique (2θ = 0–50°). Systematic absences in the data (octant $hk\bar{l}$) indicated

(9) The intensity data were processed as described in: "CAD 4 and SDP Users Manual"; Enraf-Nonius: Delft, Holland, 1978. The net intensity I is given as

$$I = \frac{K}{\mathrm{NPI}}(C - 2B)$$

where K = 20.1166 (attenuator factor), NPI = ratio of fastest possible scan rate to scan rate for the measurement, C = total count, and B = total background count. The standard deviation in the net intensity is given by

$$\sigma^2(I) = \frac{K}{\mathrm{NPI}}[C + 4B + (pI)^2]$$

where p is a factor used to downweight intense reflections. The observed structure factor amplitude F_o is given by

$$F_o = (I/Lp)^{1/2}$$

where Lp = Lorentz and polarization factors. The $\sigma(I)$'s were converted to the estimated errors in the relative structure factors $\sigma(F_o)$.

$$\sigma(F_o) = \frac{1}{2}\frac{\sigma(I)}{I}F_o$$

(10) The function minimized was $w(|F_o| - |F_c|)^2$, where $w = 1/\sigma^2(F_o)$. The unweighted and weighted residuals are defined as

$$R = (\sum||F_o| - |F_c||)/\sum|F_o|$$

$$R_w = [(\sum w(|F_o| - |F_c|)^2/(\sum|F_o|^2)]^{1/2}$$

The error in an observation of unit weight is

$$[\sum w(|F_o| - |F_c|)^2/(\mathrm{NO} - \mathrm{NV})]^{1/2}$$

where NO and NV are the number of observations and variables, respectively.

(11) Cromer, D. T.; Waber, J. T. "International Tables for X-ray Crystallography"; Kynoch Press: Birmingham, England, 1974; Vol. IV, Table 2.2.4. Cromer, D. T. *Ibid.*, Table 2.3.1.

(12) Cromer, D. T.; Ibers, J. A. "International Tables for X-ray Crystallography"; Kynoch Press: Birmingham, England, 1974; Vol. IV.

(13) The structure of $CF_3SO_3^-$ has been previously determined. See: Spencer, J. B.; Lundgren, J. O. *Acta Crystallogr., Sect. B: Struct. Crystallogr. Cryst. Chem.* **1973**, *B29*, 1923.

(14) Frenz, B. A. In "Computing in Crystallography"; Schenk, H., et al., Eds.; Delft University Press: Delft, Holland, 1978; pp 64–71.

Table II. Positional Parameters and Their Estimated Standard Deviations

atom	x	y	z	atom	x	y	z
			A. $[Cr(CNPh)_6][SO_3CF_3]$				
Cr	0.0000 (0)	0.0000 (0)	0.0000 (0)	C5B	−0.5594 (2)	0.0987 (2)	0.0954 (3)
S	0.5848 (1)	0.01906 (6)	0.5252 (1)	C6B	−0.4329 (2)	0.0793 (1)	0.1066 (3)
O1	0.6394 (2)	−0.0083 (1)	0.4335 (2)	C1C	0.2037 (2)	0.1794 (1)	0.2558 (2)
O2	0.3478 (2)	−0.0036 (1)	0.3425 (2)	C2C	0.1930 (2)	0.2422 (1)	0.1983 (3)
O3	0.5635 (2)	0.0867 (1)	0.5045 (3)	C3C	0.2563 (3)	0.2953 (1)	0.2834 (4)
N1A	−0.0203 (2)	0.08034 (11)	−0.2689 (2)	C4C	0.3282 (3)	0.2841 (1)	0.4209 (4)
N1B	−0.2759 (2)	0.05507 (9)	0.0059 (2)	C5C	0.3396 (3)	0.2225 (2)	0.4745 (4)
N1C	0.1387 (2)	0.12535 (9)	0.1729 (2)	C6C	0.2765 (3)	0.1681 (1)	0.3944 (3)
C7A	−0.0142 (2)	0.0500 (1)	−0.1697 (2)	C	0.584 (1)	0.0237 (5)	0.516 (1)
C7B	−0.1748 (2)	0.0349 (1)	−0.0047 (2)	H2A	0.0542 (0)	0.2013 (0)	−0.2750 (0)
C7C	0.0878 (2)	0.0784 (1)	0.1110 (2)	H3A	0.0354 (0)	0.2668 (0)	−0.4722 (0)
C1A	−0.0292 (2)	0.1179 (1)	−0.3864 (2)	H4A	−0.0498 (0)	0.2212 (0)	−0.6894 (0)
C2A	0.0171 (3)	0.1831 (2)	−0.3662 (3)	H5A	−0.1298 (0)	0.1163 (0)	−0.7240 (0)
C3A	0.0063 (4)	0.2215 (2)	−0.4829 (4)	H6A	−0.1092 (0)	0.0446 (0)	−0.5298 (0)
C4A	−0.0454 (4)	0.1941 (3)	−0.6113 (4)	H2B	−0.4714 (0)	0.0905 (0)	−0.2234 (0)
C5A	−0.0904 (4)	0.1316 (3)	−0.6309 (4)	H3B	−0.6845 (0)	0.1226 (0)	−0.2379 (0)
C6A	−0.0809 (4)	0.0903 (2)	−0.5166 (3)	H4B	−0.7380 (0)	0.1292 (0)	−0.0389 (0)
C1B	−0.4020 (2)	0.0763 (1)	−0.0132 (2)	H5B	−0.5833 (0)	0.1004 (0)	0.1766 (0)
C2B	−0.4941 (2)	0.0924 (1)	−0.1418 (3)	H6B	−0.3684 (0)	0.0680 (0)	0.1946 (0)
C3B	−0.6198 (3)	0.1116 (2)	−0.1497 (3)	H2C	0.1433 (0)	0.2491 (0)	0.1017 (0)
C4B	−0.6517 (2)	0.1153 (1)	−0.0322 (3)	H3C	0.2491 (0)	0.3393 (0)	0.2467 (0)
				H4C	0.3699 (0)	0.3205 (0)	0.4792 (0)
			B. $[Cr(CNPh)_6][PF_6]_2$				
Cr	0.1411 (1)	0.25640 (7)	0.05202 (8)	C2D	0.4665 (8)	0.1177 (5)	−0.0305 (6)
P1A	0.3870 (2)	0.2589 (1)	0.7870 (2)	C3D	0.5564 (8)	0.0832 (5)	−0.0162 (6)
P1B	0.2392 (2)	0.9787 (1)	0.2389 (2)	C4D	0.5765 (8)	0.0600 (5)	0.0560 (7)
F1A	0.3071 (4)	0.3154 (3)	0.7990 (4)	C5D	0.5219 (8)	0.0617 (6)	0.1233 (7)
F2A	0.3617 (6)	0.2527 (3)	0.6917 (4)	C6D	0.4337 (7)	0.0951 (5)	0.1143 (6)
F3A	0.3115 (5)	0.2012 (3)	0.8057 (4)	C1E	−0.0520 (6)	0.0690 (4)	0.0839 (5)
F4A	0.4658 (4)	0.2013 (3)	0.7778 (4)	C2E	−0.1091 (6)	0.0482 (4)	0.0180 (5)
F5A	0.4134 (5)	0.2636 (3)	0.8843 (3)	C3E	−0.1601 (6)	−0.0122 (4)	0.0283 (5)
F6A	0.4622 (5)	0.3165 (3)	0.7709 (4)	C4E	−0.1519 (6)	−0.0487 (4)	0.1002 (5)
F1B	0.2113 (5)	1.0440 (3)	0.1858 (4)	C5E	−0.0940 (7)	−0.0282 (5)	0.1643 (6)
F2B	0.1687 (5)	0.9343 (3)	0.1839 (4)	C6E	−0.0411 (7)	0.0331 (4)	0.1579 (5)
F3B	0.2666 (5)	0.9143 (3)	0.2924 (4)	C1F	0.2351 (6)	0.2388 (4)	0.3261 (5)
F4B	0.1556 (5)	0.9930 (4)	0.2971 (4)	C2F	0.2194 (7)	0.2904 (5)	0.3806 (6)
F5B	0.1799 (5)	0.4627 (4)	0.3210 (4)	C3F	0.2593 (7)	0.2854 (5)	0.4609 (6)
F6B	0.1903 (5)	0.5241 (3)	0.2074 (4)	C4F	0.3103 (7)	0.2304 (5)	0.4852 (6)
N1A	0.0023 (5)	0.3770 (3)	0.1028 (4)	C5F	0.3262 (7)	0.1790 (5)	0.4297 (6)
N1B	0.2735 (5)	0.3818 (3)	0.0070 (4)	C6F	0.2866 (7)	0.1825 (5)	0.3490 (6)
N1C	0.0777 (5)	0.2455 (3)	−0.1388 (4)	H2A	0.0483 (0)	0.5014 (0)	0.0822 (0)
N1D	0.3213 (5)	0.1597 (3)	0.0336 (4)	H3A	−0.0384 (0)	0.5998 (0)	0.1219 (0)
N1E	0.0038 (5)	0.1291 (3)	0.0754 (4)	H4A	−0.1818 (0)	0.5887 (0)	0.1880 (0)
N1F	0.2020 (5)	0.2446 (3)	0.2437 (4)	H5A	−0.2419 (0)	0.4848 (0)	0.2173 (0)
C7A	0.0467 (6)	0.3307 (4)	0.0809 (5)	H6A	−0.1605 (0)	0.3836 (0)	0.1810 (0)
C7B	0.2280 (6)	0.3350 (4)	0.0251 (5)	H2B	0.4186 (0)	0.3840 (0)	−0.0939 (0)
C7C	0.1014 (6)	0.2519 (4)	−0.0693 (5)	H3B	0.5041 (0)	0.4801 (0)	−0.1407 (0)
C7D	0.2520 (6)	0.1921 (4)	0.0355 (5)	H4B	0.4539 (0)	0.5842 (0)	−0.1045 (0)
C7E	0.0516 (6)	0.1769 (4)	0.0693 (5)	H5B	0.3371 (0)	0.6031 (0)	−0.0097 (0)
C7F	0.1777 (6)	0.2511 (4)	0.1739 (5)	H6B	0.2513 (0)	0.5084 (0)	0.0454 (0)
C1A	−0.0490 (6)	0.4353 (4)	0.1269 (5)	H2C	−0.0722 (0)	0.1798 (0)	−0.1929 (0)
C2A	−0.0118 (7)	0.4971 (5)	0.1102 (6)	H3C	−0.1250 (0)	0.1642 (0)	−0.3307 (0)
C3A	0.0630 (8)	0.5558 (5)	0.1337 (6)	H4C	−0.0461 (0)	0.2120 (0)	−0.4383 (0)
C4A	0.1467 (8)	0.5493 (5)	0.1721 (6)	H5C	0.0968 (0)	0.2700 (0)	−0.4159 (0)
C5A	0.1824 (8)	0.4887 (5)	0.1899 (7)	H6C	0.1557 (0)	0.2879 (0)	−0.2770 (0)
C6A	0.1347 (7)	0.4276 (5)	0.1681 (6)	H2D	0.4464 (0)	0.1342 (0)	0.0844 (0)
C1B	0.3270 (6)	0.4390 (4)	−0.0213 (5)	H3D	0.5996 (0)	0.0789 (0)	0.0605 (0)
C2B	0.4012 (7)	0.4280 (4)	−0.0756 (6)	H4D	0.6379 (0)	0.0390 (0)	0.0621 (0)
C3B	0.4507 (8)	0.4850 (5)	−0.1047 (6)	H5D	0.5406 (0)	0.0406 (0)	0.1749 (0)
C4B	0.4222 (7)	0.5486 (5)	0.0812 (6)	H6D	0.3921 (0)	0.1006 (0)	0.1604 (0)
C5B	0.3526 (7)	0.5584 (5)	0.0261 (6)	H2E	−0.1118 (0)	0.0766 (0)	0.0313 (0)
C6B	0.3015 (7)	0.5022 (5)	0.0062 (6)	H3E	0.2048 (0)	0.0298 (0)	0.0185 (0)
C1C	0.0485 (6)	0.2361 (4)	0.2236 (5)	H4E	0.1879 (0)	0.0900 (0)	0.1040 (0)
C2C	0.0376 (6)	0.1989 (4)	0.2377 (5)	H5E	−0.0925 (0)	0.0879 (0)	0.2130 (0)
C3C	0.0685 (6)	0.1900 (4)	0.3200 (5)	H6E	0.0082 (0)	0.0499 (0)	0.2006 (0)
C4C	0.0208 (6)	0.2173 (4)	0.3828 (5)	H2F	0.1833 (0)	0.3300 (0)	0.3633 (0)
C5C	0.0627 (7)	0.2526 (5)	0.3643 (6)	H3F	0.2503 (0)	0.3218 (0)	0.4995 (0)
C6C	0.0986 (6)	0.2631 (4)	0.2858 (5)	H4F	0.3382 (0)	0.2267 (0)	0.5408 (0)
C1D	0.4086 (6)	0.1233 (4)	0.0678 (5)	H5F	0.3627 (0)	0.1403 (0)	0.4458 (0)
				H6F	0.2968 (0)	0.1463 (0)	0.3094 (0)

Table II (*Continued*)

atom	x	y	z	atom	x	y	z
			C. $[Cr(CNPh)_6][SbCl_6]_2 \cdot CH_2Cl_2$				
Sb1	0.0000 (0)	0.00000 (0)	0.0000 (0)	C5A	−0.1370 (9)	0.4837 (7)	0.3248 (6)
Sb2	0.0000 (0)	0.22897 (5)	0.2500 (0)	C6A	−0.1466 (9)	0.5461 (7)	0.3549 (5)
Cr	−0.2500 (0)	0.7500 (0)	0.5000 (0)	C7A	−0.2468 (7)	0.6724 (5)	0.4376 (4)
Cl1A	0.0187 (2)	0.0895 (2)	−0.0702 (1)	C1B	−0.5566 (11)	0.7888 (9)	0.5000 (0)
Cl1B	0.1582 (3)	−0.0203 (3)	0.0000 (0)	C2B	−0.5948 (9)	0.7981 (8)	0.5514 (6)
Cl2A	0.0000 (0)	0.3567 (2)	0.2500 (0)	C3B	−0.6807 (11)	0.8239 (9)	0.5509 (7)
Cl2B	0.0000 (0)	0.1018 (2)	0.2500 (0)	C4B	−0.7229 (14)	0.8438 (13)	0.5000 (0)
Cl2C	0.1329 (2)	0.2302 (2)	0.1961 (2)	C7B	−0.3906 (10)	0.7529 (9)	0.5000 (0)
Cl2D	0.0864 (3)	0.2313 (2)	0.3339 (2)	C	0.5000 (0)	0.0000 (0)	0.544 (3)
Cl	0.4218 (5)	0.0452 (5)	0.5000 (0)	H2A	−0.3641 (0)	0.5432 (0)	0.3651 (0)
N1A	−0.2400 (6)	0.6268 (4)	0.4052 (3)	H3A	−0.3460 (0)	0.4405 (0)	0.3116 (0)
N1B	−0.4653 (9)	0.7661 (6)	0.5000 (0)	H4A	−0.1987 (0)	0.3969 (0)	0.2910 (0)
C1A	−0.2317 (7)	0.5674 (6)	0.3697 (4)	H5A	−0.0779 (0)	0.4688 (0)	0.3158 (0)
C2A	−0.3050 (8)	0.5278 (6)	0.3531 (5)	H6A	−0.0957 (0)	0.5763 (0)	0.3639 (0)
C3A	−0.2935 (9)	0.4662 (7)	0.3234 (6)	H2B	−0.5651 (0)	0.7842 (0)	0.5846 (0)
C4A	−0.2080 (9)	0.4419 (6)	0.3095 (5)	H3B	−0.7095 (0)	0.8406 (0)	0.5848 (0)
				H4B	−0.7831 (0)	0.8618 (0)	0.5000 (0)

either No. 37 or No. 66 as the space group. An empirical absorption correction was made. Successful solution and refinement was subsequently carried out in *Cccm* (No. 66). Examination of the Patterson function followed the placement of the two crystallographically unique Sb atoms. Sequences of least-squares refinement and Fourier and difference Fourier allowed placement of the remaining non-hydrogen atoms. Full-matrix least-squares refinement (180 variables) utilizing anisotropic temperature factors for all non-hydrogen atoms and idealized placement of the H atoms with variable isotropic temperature factors converged to give $R = 0.058$ and $R_w = 0.059$. The error in an observation of unit weight was 0.771, based on a value of 0.04 for p in the $\sigma(I)$ equation.[9]

CH_2Cl_2 of Crystallization. One disordered dichloromethane molecule per formula unit is present in the unit cell. The unique chlorine atom (Cl) lies on the mirror plane and is related to the other chlorine atom by the twofold axis. This arrangement requires the carbon atom (C) to lie on the twofold axis, but it can be disordered either above or below the mirror plane. The electron density of carbon atom C was modeled with a 50% occupancy factor in each position. Because this type of disorder is somewhat surprising,[15] an attempt was made to refine the structure in the corresponding acentric space group (*Ccc*2, No. 37). This refinement did not lead to significantly different parameters for the Cl atom nor did it lead to a well-defined C atom in CH_2Cl_2; therefore, the centric space group was used for the final calculations.

Results

Tables II–IV give the final atomic parameters, bond lengths, and bond angles determined for each structure. (Tables and figures labeled A correspond to the Cr(I) compound, B to the Cr(II) compound, and C to the Cr(III) compound.) Final values for the temperature factors and structure factors are given in the supplementary material.

$[Cr(CNPh)_6][CF_3SO_3]$. The structure of $[Cr(CNPh)_6][CF_3SO_3]$ consists of discrete $[Cr(CNPh)_6]^+$ cations and disordered $[CF_3SO_3]^-$ anions. The disorder in the $[CF_3SO_3]^-$ anion is discussed in the Experimental Section. Examination of the structural parameters suggests no interionic contacts shorter than those expected on the basis of van der Waals radii.

The Cr atom sits on the inversion center, which requires mutually trans ligands to be equivalent (sets A, B, and C labeled in the ORTEP view of the cation (Figure 1A)). The CrC_6 coordination core is very nearly octahedral with the idealized 90° C–Cr–C angles averaging 91.0 (3)°. Two of the three independent Cr–C bond lengths (ligands A and C) are nearly identical ($\sim 4\sigma$) within experimental error (1.968 (3) Å) while the third is slightly longer (1.990 (3) Å), a deviation from the other two of about 7σ. The lengthening of the Cr–C bonds on one axis may be indicative of the small Jahn–Teller distortion expected for the low-spin d^5 $^2T_{2g}$ (in O_h) ground state.[16] The average C≡N and N—C_{nng} distances of 1.159 (3) and 1.397 (3) Å show no systematic variation with ligand and are in the ranges (1.142–1.176 and 1.388–1.420 Å, respectively) normally found in complexes of the phenyl isocyanide ligand.[17] (Further discussion of the systematic trends observed in the Cr—C, C≡N, and N—C_{ring} bond lengths with metal oxidation state is deferred until a later section of this paper.)

The Cr—C≡N and C≡N—C_{nng} linkages are very near the nominal 180° values expected for phenyl isocyanide primarily functioning as a σ-donor ligand. The orientations of the phenyl rings are partially determined by the Cr site symmetry; i.e., the trans rings related by the inversion center are required to be coplanar. A pitch angle may be defined in the idealized geometry (Cr—C≡N—C_{ring} linkage strictly linear) as the angle between the phenyl ring plane normal and the plane normal defined by the $Cr(CN)_4$ square-planar unit containing the phenyl ring (i.e., the angle between the plane normal of phenyl ring A and plane normal of the $Cr(CN)_4$ plane containing ligands A and B). The values of this angle are 3.1, 25.7, and 18.9°, respectively. It is interesting to note that the axis with the shortest Cr–C bond length (a axis) is the axis with the pitch angle closest to 0° while the b axis phenyl ring with the longest Cr–C bond deviates the most from 0°. Although this may be a consequence of the effect of the phenyl ring orientation on the σ component of the Cr–C bond, more experimental (single-crystal EPR) and theoretical (MO calculations) work is needed to confirm this explanation.

$[Cr(CNPh)_6][PF_6]_2$. The ORTEP view (Figure 1B) and, more vividly, the stereoview of the $[Cr(CNPh)_6]^{2+}$ cation (Figure 2) illustrate the distortion present in this cation. Of the structures determined for the Cr(0), Cr(I), Cr(II), and Cr(III) hexakis(phenyl isocyanide) complexes, the Cr(II) compound is by far the most distorted. The structure consists of discrete $[Cr(CNPh)_6]^{2+}$ cations and PF_6^- anions with no apparent close interionic contacts. The shortest of these is the 3.197 (7) Å contact between F4B and C3D.

The Cr atom site is a general position in the unit cell, requiring no symmetry elements (i.e., the six CNPh ligands are

(15) Britton, J. D., personal communication.

(16) Cotton, F. A.; Wilkinson, G. "Advanced Inorganic Chemistry", Wiley: New York, 1980; pp 678–682. Figgis, B. N. *Trans. Faraday Soc.* **1961**, *57*, 204.

(17) Ericsson, M. S.; Jagner, S.; Lungstrom, E. *Acta Chem. Scand., Ser. A* **1980**, *A34*, 535. Mann, K. R.; DiPierro, M. J. *Cryst. Struct. Commun.* **1982**, *11*, 1049. Sim, G. A.; Sime, J. G.; Woodhouse, D. I. *Acta Crystallogr., Sect. B: Struct. Crystallogr. Cryst. Chem.* **1979**, *B35*, 2406. Mann, K. R.; Lewis, N. S.; Williams, R. M.; Gray, H. B.; Gordon, J. G., II. *Inorg. Chem.* **1978**, *17*, 828.

Table III. Selected Interatomic Distances (Å) with Their Estimated Standard Deviations

A. $[Cr(CNPh)_6][SO_3CF_3]$

		$Cr(CNPh)_6^+$	
Cr–C7A	1.964 (2)	C7C–N1C	1.156 (2)
Cr–C7B	1.990 (2)	N1A–C1A	1.393 (2)
Cr–C7C	1.971 (2)	N1B–C1B	1.397 (2)
C7A–N1A	1.165 (2)	N1C–C1C	1.400 (2)
C7B–N1B	1.156 (2)		
		Disordered[a] $CF_3SO_3^-$	
"S–C"	1.917 (14)	"S–O2"	1.328 (3)
"S–O1"	1.384 (3)	"S–O3"	1.375 (3)

B. $[Cr(CNPh)_6][PF_6]_2$

		$Cr(CNPh)_6^{2+}$	
Cr–C7A	2.021 (7)	C7D–N1D	1.154 (7)
Cr–C7B	2.011 (7)	C7E–N1E	1.154 (7)
Cr–C7C	2.011 (6)	C7F–N1F	1.167 (7)
Cr–C7D	2.013 (7)	N1A–C1A	1.401 (7)
Cr–C7E	2.019 (7)	N1B–C1B	1.425 (7)
Cr–C7F	2.009 (7)	N1C–C1C	1.433 (7)
C7A–N1A	1.157 (7)	N1D–C1D	1.409 (8)
C7B–N1B	1.156 (7)	N1E–C1E	1.421 (7)
C7C–N1C	1.160 (6)	N1F–C1F	1.392 (7)

C. $[Cr(CNPh)_6][SbCl_6]_2 \cdot CH_2Cl_2$

		$Cr(CNPh)_6^{3+}$	
Cr–C7A	2.060 (10)	C7B–N1B	1.134 (14)
Cr–C7B	2.085 (13)	N1A–C1A	1.386 (11)
C7A–N1A	1.144 (10)	N1B–C1B	1.415 (18)
		$SbCl_6^-$ 1	
Sb1–Cl1A	2.361 (2)	Sb1–Cl1B	2.373 (3)
		$SbCl_6^-$ 2	
Sb2–Cl2A	2.357 (3)	Sb2–Cl2C	2.348 (2)
Sb2–Cl2B	2.345 (4)	Sb2–Cl2D	2.366 (3)
		Disordered[a] CH_2Cl_2	
C–Cl	1.767 (33)		

[a] See Experimental Section for the description of the disorder model employed.

independent). The Cr–C distances are nearly identical (average 2.014 (7) Å) and show no apparent systematic variation with ligand position. The most striking features of the cation structure are the distortions in the C–Cr–C bond angles and the warping of the C_{nng}—N≡C—Cr—C≡N—C_{nng} units into the shape of an archer's bow.

The angular distortions in the C—N≡C—Cr—C≡N—C units are quite dramatic. The unit involving trans ligands A and D is distorted the most while the C,F and B,E ligand trans axes are distorted to a lesser but significant amount. The "90°" C–Cr–C angles (given in part B of Table IV) range from a high value of 97.0° for C7A–Cr–C7E to a low value of 83.7° for the C7A–Cr–C7B angle. The most distorted "180°" C–Cr–C angle is 169.9° (C7A–Cr–C7D) while the *least* distorted angle is the C7B–Cr–C7E angle of 175.5°.

The most concise description of the CrC_6 coordination core is octahedral, with a significant C_2 angular distortion of the C–Cr–C bond angles. The twofold pseudo symmetry axis of the cation bisects the largest "90°" C–Cr–C angle, the 97.0° C7A–Cr–C7E angle. This description of the geometry is only approximate due to the extreme warping of C—N≡C—Cr—C≡N—C axes.

The exact origins of these distortions are in some doubt; however, they are likely due to packing forces or to the electronic requirements of the Cr(II) ion. Although structural determinations of the $Cr(CNPh)_6^{2+}$ cation with different anions present in the lattice would be needed to determine the relative importance of packing and electronic effects at Cr, the latter are consistent as the cause of the structural distortion. The standard reduction potential of the $Cr(CNPh)_6^{3+}/Cr(CNPh)_6^+$ couple[1] of −0.05 V vs. AgCl/Ag indicates that the

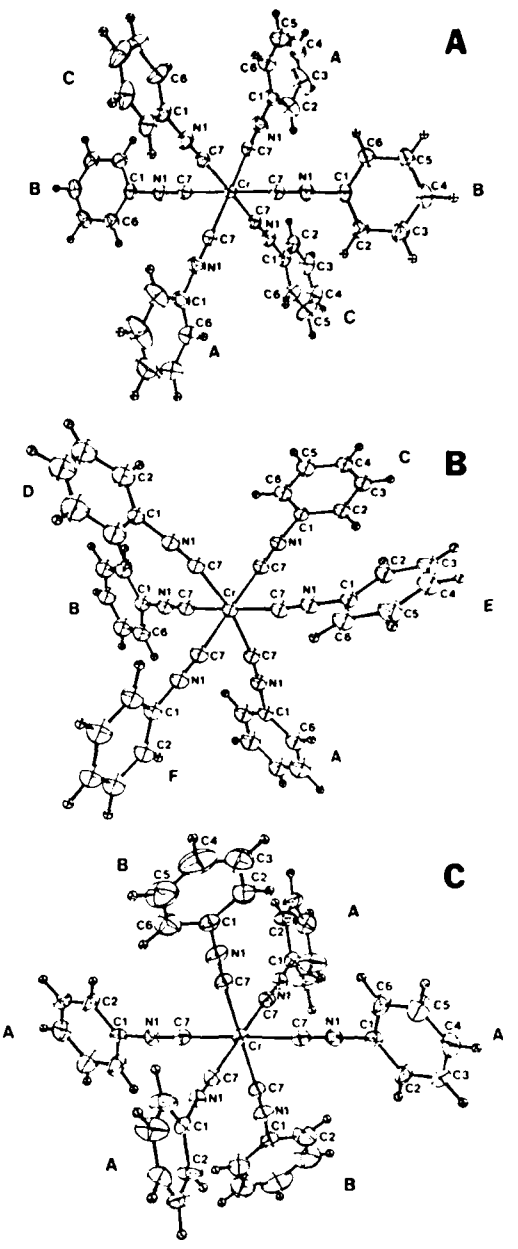

Figure 1. ORTEP view of the $Cr(CNPh)_6^+$ (A), $Cr(CNPh)_6^{2+}$ (B), and $Cr(CNPh)_6^{3+}$ (C) cations down a pseudo threefold axis, with the numbering scheme illustrated. The thermal ellipsoids for Cr, C, and N are drawn at the 50% level; H ellipsoids are arbitrarily set. Hydrogens are not labeled but are numbered as H followed by the label for the carbon atom to which it is attached. Example: H attached to C4A is numbered H4A.

six-coordinate Cr(II) center in $Cr(CNPh)_6^{2+}$ is electron deficient.[18] The six-coordinate, 16e $Cr(CNPh)_6^{2+}$ ion might be expected to show a tendency to bind a seventh ligand to attain the 18e configuration, as in the structurally characterized[18] $Cr(CN\text{-}t\text{-}Bu)_7(PF_6)_2$. Because the very weakly coordinating PF_6^- anion present in the crystal does not interact with the Cr(II) center, electron density can only be gained via distortion of the six phenyl isocyanide ligands to make them more efficient electron donators. By distortion of the C—Cr—C, Cr—C≡N, and C≡N—C angles, the overlap of the π_b C≡N orbitals with the Cr d orbitals can be increased. The improved overlap that occurs via these distortions may increase

(18) Mialki, W. S.; Wood, T. E.; Walton, R. A. *J. Am. Chem. Soc.* **1980**, *102*, 7107. Dewan, J. C.; Mialki, W. S.; Walton, R. A.; Lappert, S. J. *Ibid.* **1982**, *104*, 133.

Table IV. Selected Interatomic Angles (deg) with Their Estimated Standard Deviations

		A. $[Cr(CNPh)_6][SO_4Cl_2]$			
C7A–Cr–C7B	91.3 (1)	C7A–Cr–C7A′	180.0 (1)	Cr–C7A–N1A	178.6 (2)
C7A–Cr–C7C	88.7 (1)	C7B–Cr–C7B′	180.0 (1)	Cr–C7B–N1B	179.3 (2)
C7B–Cr–C7C	89.5 (1)	C7C–Cr–C7C′	180.0 (1)	Cr–C7C–N1C	178.1 (2)
C7A–N1A–C1A	178.6 (2)	N1A–C1A–C2A	117.9 (2)	N1A–C1A–C6A	120.4 (2)
C7B–N1B–C1B	176.4 (2)	N1B–C1B–C2B	118.6 (2)	N1B–C1B–C6B	119.9 (2)
C7C–N1C–C1C	176.1 (2)	N1C–C1C–C2C	119.8 (2)	N1C–C1C–C6C	118.7 (2)
		B. $[Cr(CNPh)_6][PI_4]_2$			
C7A–Cr–C7B	83.7 (3)	C7B–Cr–C7I	175.5 (3)	C7I–Cr–C7I	88.4 (3)
C7A–Cr–C7C	95.0 (3)	C7B–Cr–C7I	96.2 (3)	Cr–C7A–N1A	171.3 (6)
C7A–Cr–C7D	169.9 (3)	C7C–Cr–C7D	92.3 (3)	Cr–C7B–N1B	175.9 (6)
C7A–Cr–C7I	97.0 (2)	C7C–Cr–C7I	86.6 (3)	Cr–C7C–N1C	176.3 (6)
C7A–Cr–C7I	88.2 (3)	C7C–Cr–C7I	174.3 (3)	Cr–C7D–N1D	171.6 (6)
C7B–Cr–C7C	88.9 (3)	C7D–Cr–C7I	90.4 (3)	Cr–C7I–N1E	175.6 (6)
C7B–Cr–C7D	89.4 (3)	C7D–Cr–C7I	85.2 (3)	Cr–C7I–N1E	176.0 (6)
C7A–N1A–C1A	177.4 (6)	N1A–C1A–C2A	118.7 (7)	N1A–C1A–C6A	119.6 (7)
C7B–N1B–C1B	176.0 (7)	N1B–C1B–C2B	118.6 (7)	N1B–C1B–C6B	118.3 (7)
C7C–N1C–C1C	177.9 (6)	N1C–C1C–C2C	117.7 (6)	N1C–C1C–C6C	119.5 (6)
C7D–N1D–C1D	174.9 (7)	N1D–C1D–C2D	121.3 (7)	N1D–C1D–C6D	116.5 (7)
C7E–N1E–C1E	177.9 (6)	N1E–C1E–C2I	118.8 (6)	N1E–C1I–C6E	117.1 (6)
C7F–N1F–C1F	177.0 (6)	N1F–C1F–C2I	119.6 (6)	N1F–C1I–C6I	118.8 (6)
		C. $[Cr(CNPh)_6][SbCl_6]_3 \cdot CH_2Cl_2$			
C7A–Cr–C7A	91.9 (4)	C7A–N1A–C1A	175.2 (9)	C7B–N1B–C1B	175.3 (14)
C7A–Cr–C7B	92.3 (4)				
Cr–C7A–N1A	174.8 (8)	N1A–C1A–C2A	121.8 (8)	N1B–C1B–C2B	115.9 (8)
Cr–C7B–N1B	169.0 (13)	N1A–C1A–C6A	117.6 (8)		

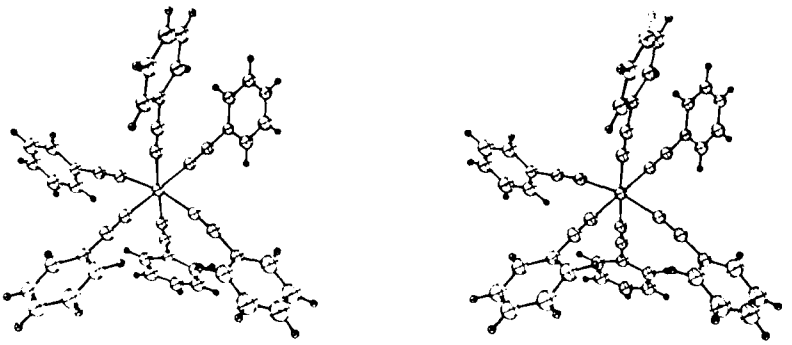

Figure 2. Stereoscopic view of the $Cr(CNPh)_6^{2+}$ cation.

the electron density at the Cr(II) center to approach that of a seven-coordinate complex. In an equivalent view, the distortion enables each CNPh ligand to donate slightly more electron density to Cr(II).

$[Cr(CNPh)_6][SbCl_6]_3 \cdot CH_2Cl_2$. The structure of $[Cr(CNPh)_6][SbCl_6]_3 \cdot CH_2Cl_2$ consists of $[Cr(CNPh)_6]^{3+}$ cations, $SbCl_6^-$ anions, and CH_2Cl_2 molecules of crystallization. There appear to be no specific interactions between these structural units (shortest contact is 3.340 Å between C1A and N1A).

The location of the cations and anions on special positions in the relatively high-symmetry *Cccm* space group imposes C_{2h} site symmetry on the $[Cr(CNPh)_6]^{3+}$ cation and one $SbCl_6^-$ anion, while the second $SbCl_6^-$ is on a site of C_s symmetry. The two crystallographically independent anions are closely octahedral with the Sb–Cl bond lengths averaging 2.360 (4) Å and the angles within 1° of the expected 90 and 180°.

The symmetry at the Cr(III) center is nearly D_{2h} (a pair of twofold axes bisect the small 88.1° C7A–Cr–C7A′ angle and the larger 91.9° C7A–Cr–C7A′, while a third twofold axis is coincident with the C7B–Cr–C7B′ vector). The $Cr(C)_6$ coordination core exhibits a marginally significant tetragonal distortion ($\sim 3\sigma$) in the Cr–C bond lengths, with long axial bonds of 2.085 (13) Å (Cr–C7B) and shorter equatorial bonds of 2.060 (10) Å (Cr–C7A). The angular distortions in the Cr–C–N and C–N–C angles are small for the A ligand (~5°) but are relatively more significant for the B ligand, particularly in the Cr–C–N linkage (11°). The effect of these angular distortions is to produce two smaller trigonal face pockets related to each other by an inversion center. The origins of these distortions as in the previously discussed Cr(II) complex are not readily apparent but again may be due in part to the extremely electron-deficient Cr(III) center in this compound (the Cr(III)/Cr(II) couple[1] is +0.73 V vs. AgCl/Ag).

Table V. Comparison of Structural Data for Several $M(CNR)_6^{n+}$ and $M(CN)_6^{m-}$ Complexes[a]

complex	electronic confign	av M–C, Å	av C–N, Å	av N–C, Å
$Cr(CNPh)_6^{0}$	t_{2g}^6	1.938 (3)	1.176 (4)	1.388 (4)
$Cr(CNPh)_6^{+}$	t_{2g}^5	1.975 (2)	1.159 (2)	1.397 (2)
$Cr(CNPh)_6^{2+}$	t_{2g}^4	2.014 (7)	1.158 (7)	1.414 (7)
$Cr(CNPh)_6^{3+}$	t_{2g}^3	2.068 (11)	1.141 (12)	1.396 (15)
$Mn(CNPh)_6^{+}$	t_{2g}^6	1.99 (2)	1.162 (6)	1.411 (6)
$Cr(CN)_6^{4-}$	t_{2g}^4	2.05 (2)	1.156 (8)	
$Cr(CN)_6^{3-}$	t_{2g}^3	2.071 (1)	1.156 (1)	

[a] Standard deviations quoted are the average of the standard deviation for the individual values; ls = low spin.

Table V summarizes crystallographic data pertinent to the discussion of the $Cr(CNPh)_6^n$ ($n = 0, 1+, 2+, 3+$) series. Data obtained in the present study and the previous determinations[3] of the $Cr(CNPh)_6^{0}$ structure indicate that the sequential oxidation of the Cr center results in a systematic *increase* in the

Discussion

Cr–C and N–C_{ring} bond lengths and a *decrease* in the C≡N bond lengths. As previously discussed[5a] in the comparison of the structural parameters for the isoelectronic $Cr(CNPh)_6^0$ and $Mn(CNPh)_6^+$ complexes, the trends observed for the Cr(0), Cr(I), Cr(II), and Cr(III) series in the Cr—C, C≡N, and N—C_{ring} bond lengths are consistent with a M $d\pi \rightarrow L\pi^*$ interaction between Cr and CNAr, which decreases with each increase in the formal Cr oxidation state. The lengthening in the Cr–C bond with an increase in the formal oxidation state of Cr is the reverse of the trend normally observed in the primarily $L(\sigma) \rightarrow M$ bonds found in coordination compounds.[19] The decrease in the C≡N bond length with an increase in formal oxidation state in the $Cr(CNPh)_6^{n+}$ series also correlates with the previous observation[2b,3] of a systematic increase in the ν(CN) infrared stretching frequency.

The anomalous properties that we have observed[3] for $Cr(CNAr)_6^{3+}$ complexes are explicable in the context of the structural studies reported here. The properties of interest are (1) the very low kinetic and thermodynamic stability of the $Cr(CNAr)_6^{3+}$ complexes relative to the more stable $Cr(CNAr)_6^{2+}$ complexes[3] (the opposite stability order is normally found) and (2) the subsequently very high Cr(III)/Cr(II) formal potentials (~+1.0 V vs. NHE) for the CNAr complexes[1] (typical Cr(III)/Cr(II) formal reduction potentials are in the range −0.4 to −1.1 V vs. NHE).[20] Clearly the inverted stability order (Cr(III) < Cr(II)) mentioned in (1) determines the positive shift in the Cr(III)/Cr(II) potential; however, the magnitude of the shift (~2.0 V)[21] between the $Cr(CN)_6^{3-}/Cr(CN)_6^{4-}$ and $Cr(CNPh)_6^{3+}/Cr(CNPh)_6^{2+}$ reduction potentials is surprising and indicates very large relative stability changes in the Cr–C bonds of the CN^- complexes compared with those of the CNPh complexes.

Although variations in Cr(III)–L bond lengths (Cr(III)–F^- = 1.906 Å;[22] Cr(III)–CH_3 = 2.300 Å[23] and in Cr(III)–L bond stability[24] are observed, stability and bond length do not always correlate. For example, the average Cr(III)–C bonds of the $Cr(CN)_6^{3-}$[25] and $Cr(CNPh)_6^{3+}$ ions are nearly identical in length (2.071 vs. 2.068 Å) but they differ many orders of magnitude in substitutional lability.[3,20,24] Previously, the hybridization of the σ_b ligand orbital and the electronegativity of the ligating atom trans to the Cr(III)–C bond have been suggested as factors important in determining Cr(III)–C bond stability.[26] Both of these factors are approximately constant in $Cr(CN)_6^{3-}$ and $Cr(CNPh)_6^{3+}$. The determining factor in the present case must be the relative energies of the carbon lone pair of CN^- compared with that of CNPh. Without measurements of the predominantly carbon lone-pair molecular orbital energies in the two ligands relative to the energy of the appropriate Cr(III) valence orbitals, we can only speculate that the energy match between the Cr(III) orbitals and the σ_b ligand orbital is considerably more favorable in the CN^- case. The lone pair on carbon in free CNPh is stabilized relative to its energy in CN^- due to the strong electron-withdrawing effect of the Ph^+ group bound to nitrogen. The CNPh carbon lone pair is able to gain very little additional stability on coordination to Cr(III) in comparison to a large stabilization gain for coordination of the CN^- carbon lone pair.

A portion of the enhanced stability of $Cr(CNPh)_6^{2+}$ relative to the less stable $Cr(CN)_6^{4-}$[20] ion must also be due to the relative energies of the Cr(II) orbitals and the ligand σ_b orbital; however, in this case an additional stabilizing factor is present. The Cr(II)–C bond in the CNPh complex is significantly shorter (2.014 vs. 2.053 Å) than in the CN^- case.[27] This shortening of the Cr(II)–C bonds in $Cr(CNPh)_6^{2+}$ may result in better σ and π overlap between the Cr(II) orbitals and the CNPh ligand orbitals.

Acknowledgment. We wish to thank Professor J. D. Britton for his expert assistance in the X-ray structure determinations and Professors J. F. Evans and H. B. Gray for helpful discussions. The X-ray diffractometer was purchased in part through funds provided by National Science Foundation Grant CHE 77-28505. This work was supported by the U.S. Army Research Office.

Registry No. A, 89463-43-4; B, 57016-36-1; C, 89463-45-6.

Supplementary Material Available: Listings of additional interatomic distances and angles, thermal parameters, and observed and calculated structure factors and stereoscopic views of the $Cr(CNPh)_6^+$ and $Cr(CNPh)_6^{3+}$ cations (41 pages). Ordering information is given on any current masthead page.

(19) For example, changes in the metal–ligand bond lengths for a number of coordination compounds in which only the $(t_{2g})^n$ configuration changes are as follows. $Fe(H_2O)_6^{n+}$, d(2+)–d(3+) = 0.14 Å: Hair, N. J.; Beattie, J. K. *Inorg. Chem.* **1977**, *16*, 245. Bauer, W. H. *Acta Crystallogr.* **1964**, *17*, 1167. Montgomery, H.; Chastain, R. V.; Nalt, J. J.; Witowska, A. M.; Lingafelter, E. C. *Ibid.* **1967**, *22*, 775. Hamilton, W. C. *Ibid.* **1962**, *15*, 353. $Ru(NH_3)_6^{n+}$, d(2+)–d(3+) = 0.04 Å: Stynes, H. C.; Ibers, J. A. *Inorg. Chem.* **1971**, *10*, 2304. $Ru(H_2O)_6^{n+}$, d(2+)–d(3+) ≈ 0.01 Å: Brunschwig, B. S.; Logan, J.; Newton, M. D.; Sutin, N. *J. Am. Chem. Soc.* **1980**, *102*, 5798 and references cited therein.

(20) E° values for $Cr(H_2O)_6^{3+}/Cr(H_2O)_6^{2+}$ and $Cr(CN)_6^{3-}/Cr(CN)_6^{2-}$ are −0.41 V vs. NHE and −1.130 V vs. NHE, respectively. Hume, D. N.; Kolthoff, I. M. *J. Am. Chem. Soc.* **1943**, *65*, 1897.

(21) We estimate that up to ~1.0 V (23 kcal/mol) of this potential shift might be due to differences in the solvation energy between the two couples, because they involve highly charged negative ions in one case and highly charged positive ions in the other case.

(22) Haegele, R.; Verschoor, W.; Babel, D. *Z. Naturforsch., B: Anorg. Chem., Org. Chem.* **1975**, *30B*, 462.

(23) Krausse, J. *Proc. Int. Conf. Coord. Chem.* **1966**, *9*, 168. Krausse, J.; Marx, G. *J. Organomet. Chem.* **1974**, *65*, 215.

(24) Taube, H. *Chem. Rev.* **1952**, *50*, 69.

(25) Iwata, M. *Acta Crystallogr., Sect. B: Struct. Crystallogr. Cryst. Chem.* **1977**, *B33*, 59.

(26) Sneedon, R. P. A. "Organochromium Compounds"; Academic Press: New York, 1975; pp 130–155.

(27) Ljungstrom, E. *Acta Chem. Scand., Ser. A* **1977**, *A31*, 104.

Inorganica Chimica Acta, 97 (1985) L51–L53

Electrochemical Redox Behaviour of the Hexakis(aryl isocyanide) Complexes of Molybdenum(0) and Tungsten(0)

DAVID A. BOHLING, KENT R. MANN

Department of Chemistry, University of Minnesota, Minneapolis, Minn. 55455, U.S.A.

STARLA ENGER, THOMAS GENNETT, MICHAEL J. WEAVER and RICHARD A. WALTON*

Department of Chemistry, Purdue University, West Lafayette, Ind. 47907, U.S.A.

Received October 10, 1984

The hexakis(alkyl isocyanide) and hexakis(aryl isocyanide) complexes of chromium, $[Cr(CNR)_6]^{n+}$ and $[Cr(CNAr)_6]^{n+}$, are noteworthy for their well-defined redox chemistry and the range of accessible stable oxidation states (n can be 3, 2, 1 or 0) [1–7]. In contrast to this situation, solutions of the hexakis(phenyl isocyanide) complexes $Mo(CNPh)_6$ and $W(CNPh)_6$ in 0.2 M tetra-n-butylammonium hexafluorophosphate(TBAH)-dichloromethane possess a reversible one-electron oxidation at $E_{1/2} \simeq +0.2$ V *vs.* SCE, and a second oxidation at $E_{p,a} = +0.48$ V (Mo), or +0.44 V (W) *vs.* SCE, that is chemically irreversible [8]. Single scan cyclic voltammetric measurements showed conclusively [8] that following the second oxidation, the $[M(CNPh)_6]^{2+}$ cations decomposed chemically, by a process that was rapid on the time scale of the electrochemical experiment. The product(s) could not be identified because it was not stable chemically. However, when the bulk electrolyses of solutions of $Mo(CNPh)_6$ and $W(CNPh)_6$ in 0.2 M TBAH–CH_2Cl_2 were carried out at a potential (+0.6 V) that was positive of the second (irreversible) oxidation then the corresponding seven coordinate dication $[M(CNPh)_7]^{2+}$ was the major product**, implying that the very reactive 16-electron six-coordinate species $[M(CNPh)_6]^{2+}$ can scavenge phenyl isocyanide. In an effort to explore the significance of these redox properties insofar as they pertain to other aryl isocyanide complexes of the types $Mo(CNAr)_6$ and $W(CNAr)_6$, and to ascertain the mechanism whereby $[M(CNAr)_7]^{2+}$ is formed by the electrochemical oxidation of $M(CNAr)_6$, we have examined further the electrochemical redox properties of $M(CNAr)_6$, with emphasis upon the more readily synthesized molybdenum complexes. Several key points emerging from these investigations are addressed herein.

TABLE I. Cyclic Voltammetric Half-Wave Potentials for $Mo(CNAr)_6$ Complexes in 0.1 M TBAH-Dichloromethane.[a]

Complex	$E_{1/2}$	$E_{p,a}$
$Mo(CNPh\text{-}4\text{-}Cl)_6$	−0.03	+0.56
$Mo(CNPh)_6$	−0.18	+0.45
	(−0.19)[b]	(+0.48)[b]
$Mo(CNPh\text{-}4\text{-}Me)_6$	−0.19	+0.47
$Mo(CNPh\text{-}2\text{-}Me)_6$	−0.20	+0.53
$Mo(CNPh\text{-}4\text{-}OMe)_6$	−0.28	+0.37
$Mo(CNPh\text{-}2,6\text{-}DIP)_6$[c]	−0.25	+0.71
$Mo(CNxylyl)_6$	−0.35[d]	+0.48[d]

[a]Data recorded at 100 mV/s *vs.* Ag/AgCl unless otherwise stated. [b]Data from ref. 8 *vs.* SCE. [c]DIP = di-iso-propyl. [d]*Vs.* SCE as reference electrode.

Solutions of a series of hexakis(aryl isocyanide) complexes of Mo(0) in 0.1 M tetra-n-butylammonium hexafluorophosphate(TBAH)-dichloromethane (Table I) were found† to exhibit cyclic voltammetric behavior essentially the same as that reported previously for $M(CNPh)_6$ (M = Mo or W) in 0.2 M TBAH–CH_2Cl_2, thereby establishing the generality of this redox behavior and emphasizing the differences that exist with the chromium analogues $[Cr(CNAr)_6]^{n+}$. Compared to the analogous $Cr(CNAr)_6$ compounds [5], only a limited correlation of the cyclic voltammetric half-wave potentials $E_{1/2}$ with Hammett σ_p and σ_o functions exists for the electrode reaction depicted in eqn. 1††. These couples (eqn. 1) are characterized

$$[Mo(CNAr)_6]^+ + e^- \longrightarrow Mo(CNAr)_6 \qquad (1)$$

by $E_{1/2}$ values in the potential range 0 to −0.3 V, peak separations of less than 100 mV and peak ratios $i_{p,c}/i_{p,a}$ equal to one in the 0.1 M TBAH-CH_2Cl_2 solvent system.

*Author to whom correspondence should be addressed.

**The species $[Mo(CNPh)_7]^{2+}$ and $[W(CNPh)_7]^{2+}$ themselves possess very characteristic and well-defined electrochemical properties, *viz.* in 0.2 M TBAH–CH_2Cl_2 a reversible one-electron oxidation at $E_{1/2} = +1.41$ V (for Mo) or +1.32 V (for W), and an irreversible two-electron reduction at $E_{p,c} = -1.12$ V (for Mo) or −1.02 V (for W) *vs.* SCE; for full details see ref. 8(b).

†These measurements were carried out at the University of Minnesota using the experimental set-up described previously [5]. All potentials are quoted relative to a Ag/AgCl reference electrode, which therefore makes them very similar, although not exactly identical to, the data presented in ref. 8, for which an SCE reference was used.

††Further details are available in D. A. Bohling, *Ph.D. Thesis*, University of Minnesota, 1984.

0020-1693/85/$3.30

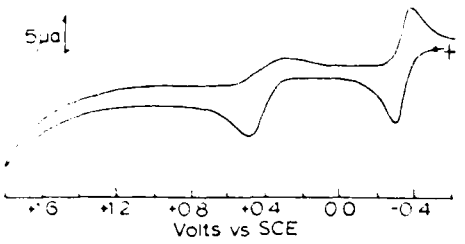

Fig. 1. Anodic–cathodic cyclic voltammogram of a solution of $Mo(CNxylyl)_6$ in 0.1 M TBAH–CH_2Cl_2 recorded at ν = 100 mV/s using a Pt-bead electrode (other experimental conditions are as described in footnote §).

In contrast to the reversible character of the +1/0 couple, the conversion of $[Mo(CNAr)_6]^+$ to $[Mo(CNAr)_6]^{2+}$ is followed in all instances by a chemical transformation that is rapid on the electrochemical time scale, thereby yielding very little response corresponding to the reverse process, at least for sweep rates up to 10 V/s. This irreversibility contrasts with the reversible nature of the $[Cr(CNAr)_6]^{2+/1+}$ couple [5]. In an attempt to identify the chemical reactions that follow the formation of $[Mo(CNAr)_6]^{2+}$, we have focused our attention upon the behavior of one such system, *viz.*, $Mo(CNxylyl)_6$ (xylyl = 2,6-dimethylphenyl), a complex that appears to be representative of the series†††.

We had noted previously [8] that following the second oxidation, *i.e.* $(Mo)^{1+} \rightarrow (Mo)^{2+}$, 'product waves' appeared in the single scan cyclic voltammograms of $M(CNPh)_6$ (M = Mo or W) at potentials more positive than +1.1 V. Similar cyclic voltammetric scans in the case of the other complexes listed in Table I confirmed that all these systems behaved in a comparable fashion. Subsequently, we have found that the appearance of these waves at potentials > +1.1 V results from the reaction of $[Mo(CNAr)_6]^{2+}$ with impurities in the solvent and/or supporting electrolyte because, as shown in Fig. 1, the single-scan cyclic voltammogram of $Mo(CNxylyl)_6$ in 0.1 M TBAH–CH_2Cl_2 is free of such waves when recourse was made to a highly purified solvent and supporting electrolyte§. For this system, the +1/0 couple was characterized by $E_{1/2}$ = −0.35 V *vs.* SCE and $i_{p,c}/i_{p,a}$ = 1, while the +2/+1 couple had $E_{p,a}$ = +0.48 V *vs.* SCE and $i_{p,c}/i_{p,a} \ll 1$ at a scan rate (ν) of 100 mV/s. Even with fast scans (up to 10 V/s) the ratio $i_{p,c}/i_{p,a}$ was much less than unity. Within the potential range +1.9 to −2.4 V, there were no other significant features discernible in the cyclic voltammogram under these experimental conditions.

Exhaustive electrolysis of solutions of $Mo(CNPh)_6$ and $W(CNPh)_6$ at potentials positive of the second (irreversible) oxidation gives seven coordinate $[Mo(CNPh)_7]^{2+}$ and $[W(CNPh)_7]^{2+}$ as the predominant chemical products [8], although the product yields were not previously determined. This behavior is typical of that found for the other $Mo(CNAr)_6$ species, as exemplified by the present results for $Mo(CNxylyl)_6$. Controlled potential electrolysis on 0.1 M TBAH–CH_2Cl_2 solutions of $Mo(CNxylyl)_6$ was conducted at 0.0 V in order to achieve complete conversion to the paramagnetic monovalent cation§§. The electrolysis was assumed concluded when only cathodic current was exhibited using a rotating platinum electrode, at which time 0.98 electron had been removed. The cation's half life is significantly

†††The complex $Mo(CNxylyl)_6$, like others of this type described in Table I, was prepared from the reaction of $Mo_2(O_2CCH_3)_4$ with excess of ArNC using a slight modification of the synthetic route described by Mann *et al.* [9]. An alternative procedure employs a sodium/mercury reduction method as proposed by Chiu *et al.* [10]. Methanol (50 ml), which had been dried over molecular sieves for two days prior to use, was added to 40 g of a 4% Na/Hg amalgam. The subsequent addition of 0.5 g of $Mo_2(O_2CCH_3)_4$ immediately produced a dark brown colored solution. Shortly thereafter, 1.0 g (7.6 mmol) of xylyl isocyanide was added. The flask was shaken for 15 min and the contents changed to a deep red color. The resulting mixture was separated from the remaining Na/Hg amalgam and cooled to 0 °C in an ice bath. The solid was filtered off, and the $Mo(CNxylyl)_6$ was extracted into diethyl ether. Evaporation of the diethyl ether extract was achieved under a stream of nitrogen gas, yield 40%. This product had identical spectroscopic (IR, NMR) and electrochemical properties to that found for samples isolated using the other procedure. Purification was effected by recrystallization from toluene using oxygen-free and anhydrous conditions. *Anal.* Calcd. for $C_{54}H_{54}MoN_6$: C, 73.45; H, 6.16. Found: C, 72.52; H, 6.61.

§The supporting electrolyte n-Bu_4NPF_6 was purified by recrystallizing it several times from absolute ethanol, followed by thorough vacuum drying. The dichloromethane solvent (Burdick and Jackson) was purified utilizing CaH_2 as the drying agent, followed by three freeze-pump-thaw cycles, and vacuum distillation (10^{-6} mm). Rigorous inert atmosphere conditions (N_2, Vacuum Atmospheres dry box) were used in all subsequent measurements. The electrochemical cell configuration used was the typical one [11], but with a double-fritted SCE reference cell to hinder the diffusion of water into the working compartment of the cell. Measurements were carried out at 25 °C using a Pt-bead electrode that had been cleaned in boiling nitric acid followed by a saturated ferrous ammonium sulfate solution. Instrumentation consisted of a PAR 173 potentiostat, a PAR 175 Universal Programmer, and a PAR 179 coulometer.

§§Electrochemically generated solutions of $[Mo(CNxylyl)_6]^+$ are, as expected, ESR-active and display a well-defined spectrum. At −150 °C, the X-band ESR spectrum is characterized by $g_\perp$ values of 2.055 and 2.006, a weak broad feature at $g_\parallel$ = 1.91 is attributable to an impurity, the intensity of which increases with time as the complex slowly decomposes.

$$Mo(CNAr)_6 \rightleftharpoons [Mo(CNAr)_6]^+ + e^- \quad (1)$$

$$[Mo(CNAr)_6]^+ \longrightarrow [Mo(CNAr)_6]^{2+} + e^- \quad (2)$$

$$[Mo(CNAr)_6]^{2+} + [Mo(CNAr)_6]^+ \longrightarrow [Mo(CNAr)_7]^{2+} + \{[Mo(CNAr)_5]^+\} \quad (3)$$

$$\{[Mo(CNAr)_5]^+\} \longrightarrow \{[Mo(CNAr)_{5-x}]^+\} + xArNC \quad (4)$$

$$[Mo(CNAr)_6]^{2+} + ArNC \longrightarrow [Mo(CNAr)_7]^{2+} \quad (5)$$

Scheme 1. Note: reaction (4) may well be solvent assisted; { } denotes an unstable and highly reactive species that has not been detected electrochemically.

greater at lower temperatures, *i.e.* $t_{1/2}^{25\,°C} \approx 30$–$60$ s and $t_{1/2}^{-40\,°C} \approx 24$ h. Our attempts to isolate analytically pure $[Mo(CNxylyl)_6]PF_6$ using $[(\eta\text{-}C_5Me_5)_2Fe]PF_6$ as the oxidant have not yet been successful.

In contrast to the reversibility of the +1/0 couple, attempts to generate the divalent $[Mo(CNxylyl)_6]^{2+}$ cation are thwarted by its rapid decomposition. Upon bulk electrolysis of solutions of $Mo(CNxylyl)_6$ at +0.80 V, ~1.50 equivalents of electrons are consumed; subsequent voltammetry of the solution showed that the only electrochemically-active product is $[Mo(CNxylyl)_7]^{2+}$ and that it is formed in ~75% yield. Its electrochemical properties are representative of this class of complex as a whole and resemble very closely the behavior of $[Mo(CNPh)_7]^{2+}$ as reported previously in ref. 8*. This coulometric measurement clearly implies that the putative, coordinatively unsaturated $[Mo(CNxylyl)_6]^{2+}$ ion scavenges for xylylNC to give the stable seven-coordinate dication and, as a consequence, a portion of the molybdenum containing-species is sacrificed. This conversion of $[Mo(CNAr)_6]^{2+}$ to $[Mo(CNAr)_7]^{2+}$ resembles that in which $[Cr(CNR)_7]^{2+}$ can be formed by the reaction of RNC with $[Cr(CNR)_6]^{2+}$ [3, 4]. A feasible mechanism is that shown in Scheme 1, where steps (3) and (5) can both lead to the formation of $[Mo(CNxylyl)_7]^{2+}$, and step (4) accounts for the 'loss' of electrochemically-active molybdenum**. Support for this mechanism comes from observing the influence of added xylylNC (varied from 0 to 20 mM) upon the electrochemical results for solutions that were ~1 mM in complex. At 0 mM xylylNC, the occurrence of the 1.50 electron count (measured relative to Mo(0)) after the second oxidation to the divalent cation (step 2) suggests that a reaction occurs with the monovalent cation (step 3). This accounts for the failure to achieve a two electron count, since $[Mo(CNAr)_6]^+$ is consumed prior to its complete conversion to $[Mo(CNAr)_6]^{2+}$. This postulate is supported by the effect of increasing the bulk concentration of free xylyl isocyanide ligand. Bulk electrolysis at +0.8 V in the presence of 2-fold and 20-fold excesses of the ligand produced an 80% and 96% yield of the seven-coordinate species with 1.7 and 2.0 electrons removed, respectively. Voltammetric procedures were utilized in determining that the first oxidation (step 1) was unaffected by this increase in ligand concentration. Clearly then, step (5) dominates, essentially to the exclusion of steps (3) and (4), when excess isocyanide ligand is added. This simple mechanism accords with previous synthetic results which showed [8] that the chemical oxidation (using $NOPF_6$) of $M(CNPh)_6$ (M = Mo or W) in the presence of excess PhNC can give high preparative yields of $[M(CNPh)_7](PF_6)_2$.

*For $[Mo(CNxylyl)_7]^{2+}$ in 0.1 M TBAH CH_2Cl_2, $E_{1/2}$ = +1.58 V, and $E_{p,c}$ = −0.97 vs. SCE. The first process corresponds to a reversible one-electron oxidation, the second to an irreversible two-electron reduction.

**Note that single scan cyclic voltammetry on solutions of $Mo(CNxylyl)_6$ does not show the presence of significant quantities of $[Mo(CNxylyl)_7]^{2+}$ (Eqn. 1). This can be attributed to the very low concentration of free xylylNC that is formed at the electrode surface and the relative slowness of step (3) on this electrochemical time scale.

Acknowledgements

Support of the National Science Foundation (Grant No. CHE82-06117 to R.A.W.) is gratefully acknowledged. We thank Dr. Charles J. Cameron and Kay A. Conner for experimental advice and assistance.

References

1 (a) P. M. Treichel and G. J. Essenmacher, *Inorg. Chem.*, *15*, 146 (1976);
(b) P. M. Treichel, D. W. Firsich and G. J. Essenmacher, *Inorg. Chem.*, *18*, 2405 (1979).
2 G. J. Essenmacher and P. M. Treichel, *Inorg. Chem.*, *16*, 800 (1977).
3 W. S. Mialki, T. E. Wood and R. A. Walton, *J. Am. Chem. Soc.*, *102*, 7105 (1980).
4 W. S. Mialki, [illegible] T. E. Wood and R. A. Walton, *Inorg. Chem.*, *21*, 480 (1982).
5 D. A. Bohling, J. F. Evans and K. R. Mann, *Inorg. Chem.*, *21*, 3546 (1982).
6 D. A. Bohling and K. R. Mann, *Inorg. Chem.*, *22*, 1561 (1983).
7 D. A. Bohling and K. R. Mann, *Inorg. Chem.*, *23*, 1426 (1984).
8 (a) D. D. Klendworth, W. W. Welters, III and R. A. Walton, *J. Organomet. Chem.*, *213*, C13 (1981);
(b) D. D. Klendworth, W. W. Welters, III and R. A. Walton, *Organometallics*, *1*, 336 (1982).
9 K. R. Mann, M. Cimolino, G. L. Geoffroy, G. S. Hammond, A. A. Orio, G. Albertin and H. B. Gray, *Inorg. Chim. Acta*, *16*, 97 (1976).
10 K. W. Chiu, C. G. Howard, G. Wilkinson, A. M. Galas and M. B. Hursthouse, *Polyhedron*, *1*, 803 (1982).
11 T. C. Zietlow, D. D. Klendworth, T. Nanry, D. J. Salmon and R. A. Walton, *Inorg. Chem.*, *20*, 947 (1981).

Reprinted from the Journal of the American Chemical Society, 1986, *108*, 1779.

Electrochemistry Studies of $[Ir(\mu\text{-pz})(COD)]_2$ in Halocarbon and Acetonitrile Solutions. Solvent Control of Sequential Electron-Transfer Thermodynamics

David C. Boyd, Gary S. Rodman, and Kent R. Mann*

Contribution from the Department of Chemistry, University of Minnesota, Minneapolis, Minnesota 55455. *Received September 3, 1985*

Abstract: Electrochemical studies of $[Ir(\mu\text{-pz})(COD)]_2$ (μ-pz = bridging pyrazolyl, COD = 1,5-cyclooctadiene) in halocarbon and CH_3CN solutions have been completed. In CH_2Cl_2 solutions, the cyclic voltammogram (CV) of $[Ir(\mu\text{-pz})(COD)]_2$ exhibits two, thermodynamically distinct one-electron oxidations. The first oxidation is quasi-reversible ($E°'_0 = +0.424$ in CH_2Cl_2/TBAH; TBAH = tetra-*n*-butylammonium hexafluorophosphate). $E°'_0$ is nearly independent of supporting anion (PF_6^-, ClO_4^-, and AsF_6^-). The second oxidation is chemically irreversible. The position of $E_{p,a}$ for the second oxidation is variable due to complexation of $[Ir(\mu\text{-pz})(COD)]_2^{2+}$ with the supporting anion. $E_{p,a}$ occurs at +0.963, +1.280, and +1.383 V with ClO_4^-, PF_6^-, and AsF_6^- as the supporting anion. Bulk electrolysis at potentials positive of the quasi-reversible oxidation results in the removal of 2.0 (1) electrons. A slow reaction on the CV time scale occurs between $[Ir(\mu\text{-pz})(COD)]_2^+$ and CH_2Cl_2 to form an $Ir^{II}Ir^{II}$-containing product. The addition of CH_3CN to CH_2Cl_2 solutions of $[Ir(\mu\text{-pz})(COD)]_2$ causes the second electrode process to shift to less positive potentials. The first wave does not shift. At $[CH_3CN] \approx 2.0$ M, the second wave merges with the first to give a single feature that corresponds to a net two-electron process. The wave corresponding to this two-electron process also shifts toward negative potentials with increasing $[CH_3CN]$. In neat CH_3CN/TBAH solutions, the two-electron oxidation process occurs at +0.262 V. Bulk electrolysis in neat CH_3CN solutions at potentials positive of the 2-electron process results in the removal of 2.0 (1) electrons. The observed shifts in electron-transfer thermodynamics arise from the strong complexation of two CH_3CN ligands with the two-electron oxidized $[Ir(\mu\text{-pz})(COD)]_2^{2+}$ complex. The potential for net two-electron-transfer chemistry from the lowest excited state of $[Ir(\mu\text{-pz})(COD)]_2$ is discussed in terms of a modified Latimer diagram.

In recent years, we have been interested in the photophysics, photochemistry, and electrochemistry of binuclear transition-metal complexes that contain d^8–d^8 chromophores.[1-9] The major thrust of these investigations has been to design and study systems that are capable of excited state multielectron-transfer reactions.

Electrochemical studies[4b] of a Rh^IRh^I system, $Rh_2(dimen)_4^{2+}$ (dimen = 1,8-diisocyanomenthane), have indicated that the ground state is in equilibrium with the two-electron oxidized form at glassy carbon electrodes. The removal of the second electron is thermodynamically more favorable than the first due to large increases in the strength of Rh–Rh and axial Rh–L bonding in the $Rh^{II}Rh^{II}$ state relative to the $Rh^{I(1.2)}Rh^{I(1.2)}$ state.

In homogeneous solutions, $[Ir(\mu\text{-pz})(COD)]_2$ (μ-pz = bridging pyrazolyl, COD = 1,5-cyclooctadiene) exhibits oxidation chemistry similar to that of $Rh_2(dimen)_4^{2+}$ and other $Rh_2(diisocyanoalkane)_4^{2+}$ cations. Excitation of the binuclear species in 1,2-dichloroethane (DCE) or dichloromethane yields net two-electron oxidation of the Ir^IIr^I core with concomitant addition of one ligand to each resulting Ir^{II} center and the formation of an $Ir^{II}Ir^{II}$ bond.[10] These reactions were suggested to occur through the intermediacy of odd-electron species that form and subsequently collapse to products during the lifetime of a solvent cage.

We now report the results of electrochemical studies that indicate that $[Ir(\mu\text{-pz})(COD)]_2$ is capable of both thermodynamically distinguishable one-electron-transfer reactions, and, under different experimental conditions, a single, net two-electron process stabilized by $Ir^{II}Ir^{II}$ and Ir^{II}–L bond formation.

Experimental Section

Synthesis. $[Ir(\mu\text{-pz})(COD)]_2$ (μ-pz = bridging pyrazolyl, COD = 1,5-cyclooctadiene) was synthesized by the method of Stobart et al.[11]

Electrochemical Measurements. All electrochemical experiments were performed with a BAS 100 electrochemical analyzer.

Cyclic voltammetry (CV) and chronocoulometry (CC) were performed at 20 ± 2 °C with a normal three-electrode configuration consisting of a highly polished glassy-carbon-disk working electrode ($A = 0.07$ cm²) and a Ag/Cl⁻/Ag reference electrode containing 1.0 M KCl. The working compartment of the electrochemical cell was separated from the reference compartment by a modified Luggin capillary. All three compartments contained a 0.1 M solution of the supporting electrolyte.

Table I. Potentials Measured for the Oxidations of $[Ir(\mu\text{-pz})(COD)]_2$ and $FeCp_2$ in Halocarbon Solutions as a Function of Supporting Electrolyte

solvent/supporting anion	$E°'_0$[a]	$E_{p,a}$[b]	$E_{p,c}$[c]	$FeCp_2^+/FeCp_2$[d]
CH_2Cl_2/TBA⁺ClO_4^-	+0.473	+0.963	+0.849	+0.505
CH_2Cl_2/TBA⁺PF_6^-	+0.424	+1.280		+0.460
CH_2Cl_2/TBA⁺PF_6^-	+0.428	+1.185	+1.080	+0.470
CH_2Cl_2/TBA⁺AsF_6^-	+0.420	+1.383		+0.447

[a] Formal potential for the $[Ir(\mu\text{-pz})(COD)]_2^+/[Ir(\mu\text{-pz})(COD)]_2$ couple. [b] Anodic peak potential for the oxidation of $[Ir(\mu\text{-pz})(COD)]_2^+$ to $[Ir(\mu\text{-pz})(COD)]_2^{2+}$. [c] Cathodic return peak potential for the reduction of $[Ir(\mu\text{-pz})(COD)]_2^{2+}$ to $[Ir(\mu\text{-pz})(COD)]_2^+$. [d] Observed potential for the $FeCl_2^+/FeCp_2$ couple.

Bulk electrolyses were performed by substituting a Pt-mesh electrode for the glassy carbon electrode in the cell described above. Linear sweep voltammetry (LSV) was utilized with a pyrolytic graphite rotating disk electrode (RDE) (Pine Instruments) of area 0.53 cm² to obtain the characteristic i vs. E curves under various experimental conditions.

The acetonitrile, dichloromethane, 1,2-dichloroethane (Burdick & Jackson), and supporting electrolytes tetrabutylammonium hexafluoro-

* To whom correspondence should be addressed.

(1) Mann, K. R.; Lewis, N. S.; Miskowski, V. M.; Erwin, D. K.; Hammond, G. S.; Gray, H. B. *J. Am. Chem. Soc.* **1977**, *99*, 5525.
(2) Miskowski, V. M.; Mann, K. R.; Gray, H. B.; Milder, S. J.; Hammond, G. S.; Ryason, P. R. *J. Am. Chem. Soc.* **1979**, *101*, 4383.
(3) Gray, H. B.; Miskowski, V. M.; Milder, S. J.; Smith, T. P.; Maverick, A. W.; Buhr, J. D.; Gladfelter, W. L.; Sigal, I. S.; Mann, K. R. *Fundamental Research on Homogeneous Catalysis*; Tsutsui, M., Ed.; Plenum: New York, 1979; Vol. 3, p 819.
(4) Gray, H. B.; Mann, K. R.; Lewis, N. S.; Thich, J. A.; Richman, R. M. *Adv. Chem. Ser.* **1978**, *168*, 44.
(5) Miskowski, V. M.; Nobinger, G. L.; Kliger, K. S.; Hammond, G. S.; Lewis, N. S.; Mann, K. R.; Gray, H. B. *J. Am. Chem. Soc.* **1978**, *100*, 485.
(6) Mann, K. R.; Gray, H. B. *Adv. Chem. Ser.* **1979**, *173*, 225.
(7) Mann, K. R.; Parkinson, B. A. *Inorg. Chem.* **1981**, *20*, 3921.
(8) (a) Womack, D. R.; Enlow, P. D.; Woods, C. *Inorg. Chem.* **1983**, *22*, 2653. (b) Rhodes, M. R.; Mann, K. R. *Inorg. Chem.* **1984**, *23*, 2053. (c) Enlow, P. D.; Woods, C. *Inorg. Chem.* **1985**, *24*, 1273.
(9) Rodman, G. S.; Mann, K. R. *Inorg. Chem.* **1985**, *24*, 3507.
(10) Caspar, J. V.; Gray, H. B. *J. Am. Chem. Soc.* **1984**, *106*, 3029.
(11) Coleman, A. W.; Eadie, D. T.; Stobart, S. R.; Zaworotko, M. J.; Atwood, J. L. *J. Am. Chem. Soc.* **1982**, *104*, 922.

phosphate (TBAH), tetrabutylammonium perchlorate (TBAP) (Southwestern Analytical Chemicals, Inc.), and tetrabutylammonium hexafluoroarsenate (TBAHA)[12] were used without further purification.

Electrolyte solutions were prepared and stored over 80–200-mesh activated alumina (Fisher Scientific Co.) or activated 4-Å molecular sieves prior to use in the experiments. In all cases, working solutions were prepared by recording background cyclic voltammograms of 25.0 mL of the electrolyte solution before addition of the complex. The working compartment of the cell was bubbled with solvent-saturated argon to deaerate the solution.

Potentials are reported vs. aqueous AgCl/Ag and are not corrected for the junction potential. To allow future corrections and the correlation of these data with those of other workers, we have measured the $E°'$ for the ferrocenium/ferrocene couple[13] under conditions identical with those used for the Ir complex. These values are given in Table I. In CH_3CN/TBAH, $E°' = +0.410$ V. The standard current convention is used (anodic currents are negative).

The iR compensation circuit available on the BAS-100 was not used in any of the electrochemical studies. Rather, the effects of uncompensated cell resistance were assessed for the LSV studies at the RDE by determining the LSV response for $FeCp_2$. The slopes of the E vs. $\log\{(i_{c,l} - i)/(i - i_{a,l})\}$ plots[14] for the oxidation of $FeCp_2$ were 0.092 and 0.067 V for CH_2Cl_2/TBAH and CH_3CN/TBAH solutions, respectively.

Data Handling. Digital data collected on the BAS-100 electrochemical system were down loaded to a Zenith-150 microcomputer. All data analyses were performed by utilizing the commercially available LOTUS-123 computer program.

Sequential Additions of CH_3CN. Sequential additions of neat CH_3CN/TBAH, 0.76 or 1.9 M CH_3CN/TBAH in CH_2Cl_2/TBAH, were made with a microliter syringe. Analysis of the data assumed that the quasi-reversible CV waves observed for the various conditions studied approximated true Nernstian conditions. We believe that the successful fitting of experimental data to predicted linear relationships justifies this assumption.

Case A. (The cases are summarized in Table II.) Data were analyzed by using

$$\log([\text{complexed}]/[\text{uncomplexed}]) = p \log [CH_3CN] + \log K_1 \quad (1)$$

where

$$\log([\text{complexed}]/[\text{uncomplexed}] \approx \log (i_a)/(i_{a,l} - i_a)] \quad (2)$$

$$\log [CH_3CN] = \log ([CH_3CN]_{\text{added}} - p[\text{complexed}]) \quad (3)$$

$i_{a,l}$ = limiting anodic peak current for the oxidation of $[Ir(\mu\text{-pz})(COD)]_2^+$ that grows in when CH_3CN is added (CV experiment; $\nu = 100$ mV/s)

i_a = anodic peak current at a given CH_3CN concentration

$$[\text{complexed}] = [[Ir(\mu\text{-pz})(COD)]_2(CH_3CN)_p^{2+}]$$

$$[\text{uncomplexed}] = [[Ir(\mu\text{-pz})(COD)]_2^{2+}]$$

$$K_1 = \frac{[[Ir(\mu\text{-pz})(COD)]_2(CH_3CN)_p^{2+}]}{[[Ir(\mu\text{-pz})(COD)]_2^{2+}][CH_3CN]^p} \quad (4)$$

Case B. Data were analyzed by using eq 5[15] where $E_{p,a}$ is the anodic peak potential for the second oxidation wave, $E_{2,1}°'$ is the formal potential for the reverse of eq 7, K_1K_2 is the overall formation constant for equilibrium 21, and q is the total number of CH_3CN ligands bound by the two-electron oxidized form.

$$E_{p,a} = E_{2,1}°' - (2.303RT/nF)[\log K_1K_2 + q \log [CH_3CN]] + (\Delta E_{\text{solvation}} + \Delta E_{\text{junction}} + 0.029) \quad (5)$$

The next two ΔE terms in eq 5 are contributions to the intercept that arise from changes in solvation energy and junction potential. The last term corrects the right side of the equation to correspond to the anodic peak potential. All diffusion coefficients for Ir-containing species are assumed to be identical, and complexation of CH_3CN by the one-electron oxidized form is assumed negligible (see Results and Discussion section).

Table II. Summary of $[Ir(\mu\text{-pz})(COD)]_2$ CV Behavior in CH_2Cl_2/CH_3CN Mixtures

case	solution characteristics	CV characteristics
A	$[CH_3CN]/[[Ir(\mu\text{-pz})(COD)]_2] \le 2$; $0 < [CH_3CN] < 10$ mM; $[Ir(\mu\text{-pz})(COD)]_2 \approx 5$ mM	three waves; $E_{1/0}°$ independent of $[CH_3CN]$; $E_{p,a}$ at 1.28 V gradually disappears while the current of $E_{p,a}$ at +0.849 V gradually increases with an increase in $[CH_3CN]$
B	$[CH_3CN]/[[Ir(\mu\text{-pz})(COD)]_2] > 2$; $[[Ir(\mu\text{-pz})(COD)]_2] = 0.5$ mM; $[CH_3CN] < 0.2$ M	two quasi-reversible waves; $E_{1/0}°$ independent of $[CH_3CN]$; $E_{2/1}$ shifts to less positive potentials with an increase in $[CH_3CN]$
C	$[CH_3CN]/[[Ir(\mu\text{-pz})(COD)]_2] \gg 2$; $[[Ir(\mu\text{-pz})(COD)]_2] = 0.5$ mM; 2.0 M < $[CH_3CN]$ < 19.9 M	single $2e^-$ wave; the wave gradually shifts to less positive potentials with an increase in $[CH_3CN]$

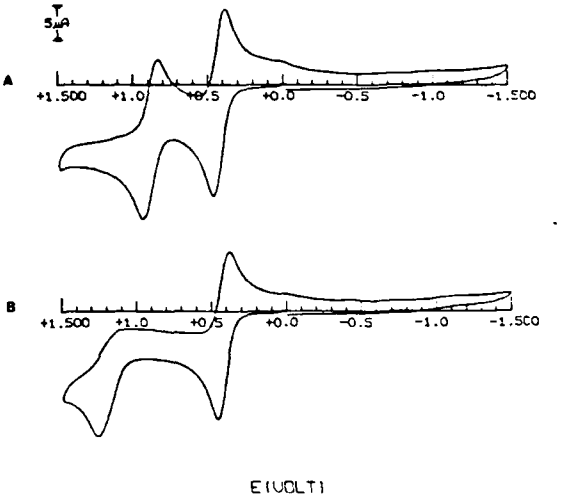

Figure 1. Cyclic voltammograms ($\nu = 100$ mV/s) at a stationary glassy carbon electrode of 0.80 mM $[Ir(\mu\text{-pz})(COD)]_2$ in CH_2Cl_2/TBAH. Curve A results from "moist" conditions; curve B results after addition of activated 4-Å molecular sieves followed by 5 min of stirring.

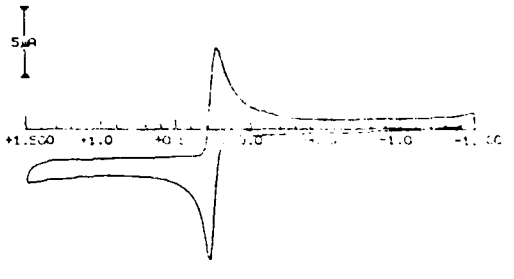

Figure 2. Cyclic voltammogram ($\nu = 50$ mV/s) at a stationary glassy carbon electrode of 0.27 mM $[Ir(\mu\text{-pz})(COD)]_2$ in CH_3CN/TBAH.

Results and Discussion

The cyclic voltammograms of $[Ir(\mu\text{-pz})(COD)]_2$ in dry CH_2Cl_2/TBAH (TBAH = tetra-*n*-butylammonium hexafluorophosphate) and CH_3CN/TBAH are shown in Figures 1B and 2, respectively.

(12) Schrenk, J. L.; Palazzotto, M. C.; Mann, K. R. *Inorg. Chem.* **1983**, *22*, 4047.

(13) (a) Gagne, R. R.; Koval, C. A.; Kisensky, G. C. *Inorg. Chem.* **1980**, *19*, 2854. (b) Koepp, H. M.; Wendt, H.; Strehlow, H. *Z. Z. Elektrochem.* **1960**, *64*, 483.

(14) Bard, A. J.; Faulkner, L. R. *Electrochemical Methods*; Wiley: New York, 1980; p 290.

(15) This equation is a more specific version of one used previously to analyze similar data: Kadish, K. M.; Bottomley, L. A.; Cheng, J. S. *J. Am. Chem. Soc.* **1978**, *100*, 2731.

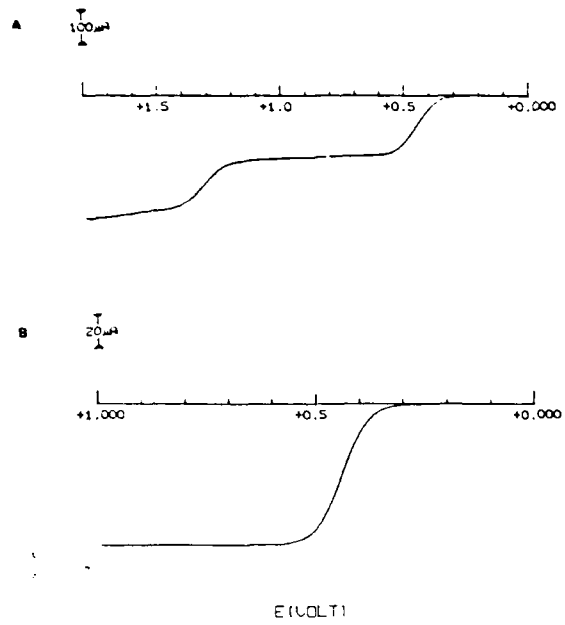

Figure 3. (A) Plot of the LSV (current (i) vs. potential (E)) at a pyrolytic graphite RDE (ω = 52.36 rad/s; ν = 20 mV/s) of a 0.83 mM solution of $[Ir(\mu\text{-pz})(COD)]_2$ in CH_2Cl_2/TBAH. (B) Plot of the LSV (current (i) vs. potential (E)) at a pyrolytic graphite RDE (ω = 10.47 rad/s; ν = 1 mV/s) of a 0.27 mM solution of $[Ir(\mu\text{-pz})(COD)]_2$ in CH_3CN/TBAH.

Two oxidation processes are observed in the CH_2Cl_2 solution, while a single process is observed in CH_3CN solutions. The behavior of $[Ir(\mu\text{-pz})(COD)]_2$ in CH_2Cl_2 solutions will be discussed first.

$[Ir(\mu\text{-pz})(COD)]_2$ in CH_2Cl_2 Solutions. In carefully dried CH_2Cl_2/TBAH solutions, two oxidative electrode processes occur between 0.0 V and the solvent limit (~2.0 V). The first process occurs at +0.424 V and corresponds to a one-electron process ($i_{p,c}/i_{p,a}$ = 1.00 ± 0.02, ΔE_p = 148 mV at ν = 100 mV/s). A potential step experiment from 0.0 to 0.8 V yielded a linear (correlation coefficient = 0.9999) Anson plot (Q vs. $t^{1/2}$)[16] with a slope of 29.6 $C/s^{1/2}$ for 1.22 mM $[Ir(\mu\text{-pz})(COD)]_2$. From the slope, a value of $nD^{1/2}$ of 3.19×10^{-3} $cm/s^{1/2}$ was obtained. A calculation[17] of the diffusion coefficient from the molecular volume and the Stokes–Einstein equation gave $D = 1.03 \times 10^{-5}$ cm^2/s, in excellent agreement with the experimentally determined value $D = 1.02 \times 10^{-5}$ cm^2/s if n is assumed to be 1.

As a further indication of the nature of the electrode process, the LSV was obtained at the RDE with ν = 1 mV/s and ω = 10.47 rad/s (Figure 3A). The plot of E vs. $\log [i_{c,l} - i)/(i - i_{a,l})]$ (where $i_{c,l}$ and $i_{a,l}$ are the limiting cathodic and anodic currents, respectively)[4] shown in Figure 4 is linear and yields an intercept ($E^{\circ\prime}$) of +0.439 V and a slope of 0.072 V. The deviation of the slope from the 0.057 V expected for a perfectly Nernstian system is consistent with some uncompensated cell resistance and the value of 0.092 V determined for the $FeCp_2^{+/0}$ couple under identical conditions. All of the data are consistent with a quasi-reversible, one-electron designation for this electrode process.

Bulk electrolysis at +0.6 V (positive of the first one-electron process) of carefully dried solutions of $[Ir(\mu\text{-pz})(COD)]_2$ in either CH_2Cl_2/TBAH or CH_2Cl_2/TBAP gave an n value of 2.0 and resulted in the formation of red solutions. CV's of these solutions

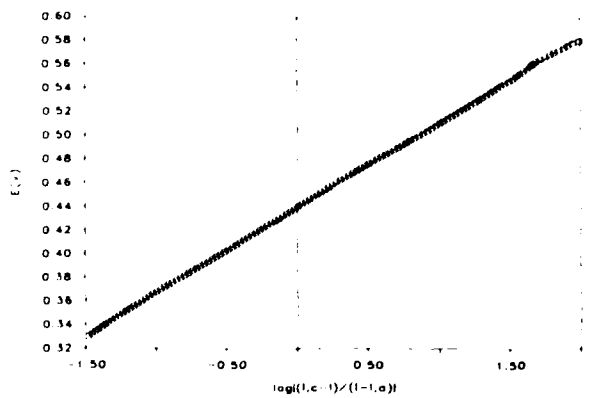

Figure 4. Plot of potential (E) vs. $\log [(i_{c,l} - i)/(i - i_{a,l})]$ for the first oxidative electrode process exhibited by a 0.75 mM solution of $[Ir(\mu\text{-pz})(COD)]_2$ in CH_2Cl_2/TBAH. $i_{c,l}$ and $i_{a,l}$ are the limiting cathodic and anodic currents observed in the LSV (Figure 3A) obtained at a pyrolytic graphite RDE with ω = 10.47 rad/s and ν = 1 mV/s. Experimental points are presented as squares. The least-squares line has slope = +0.072 V and intercept = +0.439 V.

after electrolysis indicated that a chemical reaction, slow on the CV time scale, had occurred to produce an $Ir^{II}Ir^{II}$ compound. The electronic spectrum of this species produced by bulk electrolysis at potentials positive of the n = 1 electrode process is nearly identical with the published electronic spectrum of the CH_2Cl_2 oxidative addition product, $[Ir(\mu\text{-pz})(COD)]_2(CH_2Cl)(Cl)$.[10]

The formation of a *two*-electron, oxidative addition product from the $[Ir(\mu\text{-pz})(COD)]_2^+$ species formed via the n = 1 electrode reaction may have mechanistic implications in the previously studied photochemical oxidative addition of CH_2Cl_2 to $[Ir(\mu\text{-pz})(COD)]_2$.[10] More detailed studies to determine the organic products and the mechanism of this reaction under electrochemical conditions will be reported in a separate study.

The second electrode process that occurs at $E_{p,a}$ = +1.28 V ($E_{p,a}$ is the anodic peak potential) in CH_2Cl_2/TBAH solution is *not* chemically reversible ($i_{p,c}/i_{p,a}$ = 0 at ν = 100 mV/s) but again corresponds to a one-electron electrode process on the CV time scale. A potential step from 0.0 to +1.5 V across both one-electron oxidations yields an Anson plot with a slope of 59.9 $C/s^{1/2}$, 2.02 times that observed for the 0.0 to +0.8 V step across only the first wave. The analysis of the LSV–RDE curve gives a linear plot of E vs. $\log [(i_{c,l} - i)/(i - i_{a,l})]$ with slope = +0.096 V and intercept of +1.26 V.

Some degree of chemical irreversibility in the electrochemical response of other d^8–d^8 systems has been previously noted.[5] As before, the chemical irreversibility is due to the rapid addition of solvent molecules or supporting anions to the ends of the doubly oxidized binuclear unit:

$$[Ir(\mu\text{-pz})(COD)]_2 \rightarrow e^- + [Ir(\mu\text{-pz})(COD)]_2^+ \quad (6)$$

$$[Ir(\mu\text{-pz})(COD)]_2^+ \rightarrow e^- + [Ir(\mu\text{-pz})(COD)]_2^{2+} \quad (7)$$

$$[Ir(\mu\text{-pz})(COD)]_2^{2+} + 2X^- \rightarrow [Ir(\mu\text{-pz})(COD)]_2X_2 \quad (8)$$

The position and reversibility of $E_{p,a}$ for the second oxidation is very sensitive to the supporting anion and the presence of other ligands (H_2O and CH_3CN). In Table I, the position of $E_{p,a}$ for the second oxidation, $E_{1/2}^{\circ\prime}$ and $E^{\circ\prime}$ for $FeCp_2^{+/0}$, $FeCp_2$ as a function of the supporting anion are given. The shifts reported for $E_{p,a}$ are too large to be the result of junction potential changes. In the presence of ClO_4^-, a more coordinating anion than PF_6^-, $E_{p,a}$ occurs at +0.963 V and $i_{p,c}/i_{p,a}$ = 0.55 at ν = 100 mV/s, while in the presence of AsF_6^-, $E_{p,a}$ occurs at +1.383 V. The relative stabilization of $[Ir(\mu\text{-pz})(COD)]_2^{2+}$ by X$^-$ ($ClO_4^- > PF_6^- > AsF_6^-$) is in the order of their coordinating ability.[18] It is

(16) Bard, A. J.; Faulkner, L. R. *Electrochemical Methods*; Wiley: New York, 1980; p 200.

(17) Calculated values for the diffusion coefficients of $[Ir(\mu\text{-pz})(COD)]_2$ were obtained from the Stokes–Einstein equation: D (cm^2/s) = $(1 \times 10^7)(RT/6\pi r\eta N)$ where R = gas constant, T = absolute temperature, r = molecular radius (cm), η = solvent viscosity (P), and N = Avogadro's number. The molecular radius, r, was estimated to be 4.962×10^{-8} cm based on the observed molecular volume taken from crystal structure data in ref 11. Viscosity values of 4.21×10^{-3} and 3.45×10^{-3} P for CH_2Cl_2 and CH_3CN were employed.

(18) BF_4^-, ClO_4^-, PF_6^-, and most recently SbF_6^- have all been found to form complexes: Mayfield, H. G.; Bull, W. E. *J. Chem. Soc. A* **1971**, 2279. And: Hersh, W. H. *J. Am. Chem. Soc.* **1985**, *107*, 4599. On the basis of the acidities of HPF_6 and $HAsF_6$, the ordering of "coordination ability" should be $ClO_4^- > PF_6^- > AsF_6^-$. Clifford, A. F.; Beachell, H. C.; Jack, W. M. *J. Inorg. Nucl. Chem.* **1957**, *5*.

Scheme I. Direct 2e⁻ Transfer

$$[Ir(\mu\text{-pz})(COD)]_2 \xrightarrow{k_{het}} [Ir(\mu\text{-pz})(COD)]_2^{2+} + 2e^- \quad \text{rate determining step} \tag{10}$$

$$[Ir(\mu\text{-pz})(COD)]_2^{2+} + qCH_3CN \rightarrow [Ir(\mu\text{-pz})(COD)]_2(CH_3CN)_q^{2+} \quad \text{rapid, following step} \tag{11}$$

Scheme II. Half Regeneration

$$[Ir(\mu\text{-pz})(COD)]_2 \xrightarrow{k_{het}} [Ir(\mu\text{-pz})(COD)]_2^{+} + e^- \tag{12}$$

$$[Ir(\mu\text{-pz})(COD)]_2^{+} + qCH_3CN \rightarrow [Ir(\mu\text{-pz})(COD)]_2(CH_3CN)_q^{+} \tag{13}$$

$$[Ir(\mu\text{-pz})(COD)]_2(CH_3CN)_q^{+} + [Ir(\mu\text{-pz})(COD)]_2^{+} \rightleftharpoons [Ir(\mu\text{-pz})(COD)]_2(CH_3CN)_q^{2+} + [Ir(\mu\text{-pz})(COD)]_2 \tag{14}$$

Scheme III. Sequential 1e⁻ Transfer

$$[Ir(\mu\text{-pz})(COD)]_2 \xrightarrow{k_{het}} [Ir(\mu\text{-pz})(COD)]_2^{+} + e^- \tag{15}$$

$$[Ir(\mu\text{-pz})(COD)]_2^{+} + qCH_3CN \rightarrow [Ir(\mu\text{-pz})(COD)]_2(CH_3CN)_q^{+} \tag{16}$$

$$[Ir(\mu\text{-pz})(COD)]_2(CH_3CN)_q^{+} \xrightarrow{k_{het}} [Ir(\mu\text{-pz})(COD)]_2(CH_3CN)_q^{2+} + e^- \tag{17}$$

interesting to note that $E^{\circ\prime}_1{}_0$ for the quasi-reversible first process is nearly invariant to changes in supporting anion when allowance for junction potential changes is made. The small changes that do occur are most likely due to small changes in the relative solvation energies for the neutral, reduced form or weak, ion-pairing interactions with the unipositive, one-electron oxidized form.[5b]

The strong complexing ability of $[Ir(\mu\text{-pz})(COD)]_2^{2+}$ is further illustrated by the appearance of CV's in the presence of water. Millimolar amounts of water in these CH_2Cl_2 solutions[19] cause large shifts in the position of $E_{p,a}$ and change the chemical reversibility of the 2/1 couple. Figure 1 shows the CV of $[Ir(\mu\text{-pz})(COD)]_2$ in "moist" CH_2Cl_2/TBAH solution (1A) followed by addition of activated 4-Å molecular sieves (1B). With water in the solution, $E_{p,a}$ is shifted to less positive potentials (+0.931 V) and the coupled return peak $E_{p,c}$ is quite evident. Under these "moist" conditions, the peak current ratio $i_{p,c}/i_{p,a}$ approaches 1.0 and ΔE_p is 104 mV, suggestive of quasi-reversible behavior. As the solution is stirred and the 4-Å sieves dry the solution, $i_{p,c}$ gradually decreases and $E_{p,a}$ shifts to the position reported for "dry" conditions in Table I.

The changes in the CV produced by the presence of small amounts of water are consistent with rapid and reversible complexation of water by the two-electron oxidized form:

$$[Ir(\mu\text{-pz})(COD)]_2^{2+} + qH_2O \rightleftharpoons [Ir(\mu\text{-pz})(COD)]_2(H_2O)_q^{2+} \tag{9}$$

This description of the effect of water is favored over one that involves the catalysis of the anion complexation/decomplexation equilibrium because water effects CH_2Cl_2 solutions of the other supporting anions in a similar way and the addition of CH_3CN to CH_2Cl_2 solutions (vide infra) has an analogous effect.

$[Ir(\mu\text{-pz})(COD)]_2$ in CH_3CN Solutions. A single oxidative process is observed between 0.0 V and the solvent limit in the CV for 0.30 mM $[Ir(\mu\text{-pz})(COD)]_2$ in CH_3CN/TBAH solutions (Figure 2) at $E^{\circ\prime}$ = +0.262 V. The process shows a high degree of chemical reversibility ($i_{p,c}/i_{p,a}$ = 1.00 ± 0.05) in the range of scan rates studied. At scan rates of 100 mV/s, ΔE_p = 36 mV, much *less* than the 57 mV expected for a Nernstian 1 e⁻ electrode process. An LSV scan obtained at the RDE for a 0.27 mM CH_3CN/TBAH solution (ν = 1 mV/s and ω = 104.7 rad/s) is shown in Figure 3B. The plot of E vs. $\log[(i_{l,a} - i)/(i - i_{l,c})]$ for this LSV ($E_{1/2,a}$ > +0.22 V) has a slope of +0.046 V and an intercept of +0.260 V. The magnitude of the slope is consistent with a net two-electron electrode process.

Chronocoulometry experiments conducted on 0.27 mM solutions with a potential step from +0.0 to +0.5 V gave a linear Anson plot with a slope of 14.7 $C/s^{1/2}$ for a 1.0-s step. From this slope, a $nD^{1/2}$ value of 7.1×10^{-3} $cm/s^{1/2}$ is obtained. The Stokes–Einstein equation predicts[17] a value of D for CH_3CN solutions of 1.25×10^{-5} cm^2/s. With the assumption that n = 2, an experimental value of D of 1.26×10^{-5} cm^2/s is calculated, in excellent agreement with the theoretical estimate.

Bulk electrolysis (BE) of the orange CH_3CN solution results in a color change to yellow with concomitant removal of two electrons per $[Ir(\mu\text{-pz})(COD)]_2$ unit. Addition of slightly more than 2 equiv of benzyltriethylammonium chloride to the yellow solution results in an instantaneous color change to a yellow-brown solution, which has identical UV–vis spectral features to the previously characterized[10] binuclear Ir(II) compound $[Ir(\mu\text{-pz})(COD)Cl]_2$.

All of these experiments are consistent with the occurrence of a net 2e⁻ oxidation of $[Ir(\mu\text{-pz})(COD)]_2$ in acetonitrile solutions on the CV, CC, and BE time scales. Several different mechanisms can lead to the observation of a net two-electron process in CV, CC, LSV–RDE, and BE experiments, but only mechanisms consistent with the experimental data need be considered. Mechanisms[20] that meet these criteria are direct two-electron transfer at the electrode (E), first-order half regeneration (EC), and two sequential, one-electron transfers with an intereceding chemical step (ECE). The most likely nuances of these possible mechanisms are outlined in Schemes I–III, with step 13 first-order and rate-determining.

The invariance of the CC n value of 2 over the range of step-times available with our equipment (20 ms to 1 s) requires that any reactions preceding or at the rate-limiting step are fast on the millisecond time scale. The n value of 2 also rules out mechanisms that are second-order with respect to $[Ir(\mu\text{-pz})(COD)]_2^{+}$ or its complexes.[21] Specifically, a rate-determining step involving the classical second-order disproportionation of the form

$$2[Ir(\mu\text{-pz})(COD)]_2^{+} \rightarrow [Ir(\mu\text{-pz})(COD)]_2 + [Ir(\mu\text{-pz})(COD)]_2^{2+} \tag{18}$$

(19) The solubility of water in dichloromethane is reported to be 0.24% by weight at 20 °C (Burdick & Jackson Solvent Guide). This represents an approximately 0.13 M solution. Our "moist" solutions have water concentrations well below this concentration.

(20) E = electrochemical step; C = chemical step. By example, an ECE mechanism then is $A \overset{+}{\underset{-}{\rightleftharpoons}} e^- + A^+ \rightarrow B^+ \overset{+}{\underset{-}{\rightleftharpoons}} B^{2+} + e^-$. A brief discussion of the effect chemical reactions have on CV and CC experiments may be found in: Bard, A. J.; Faulkner, L. R. *Electrochemical Methods*; Wiley: New York, 1980; pp 429–485. Two papers that discuss the effect of EC and ECE mechanisms on CV experiments have been published: Nadjo, L.; Saveant, J. M. *Electroanal. Chem. Interfacial Electrochem.* **1973**, *48*, 113; Mastragostino, M.; Nadjo, L.; Saveant, J. M. *Electrochim. Acta* **1978**, *23*, 721.

(21) Fractional n values are obtained in CC experiments for ECE mechanisms where the rate-limiting step for the transfer of the second electron is controlled by a second-order process. In this case n = 1.58; see: Lindberg, S. W. In *Electroanalytical Chemistry*; Bard, A. J., Ed.; Marcel Dekker: New York, 1969; Vol. III, p 199.

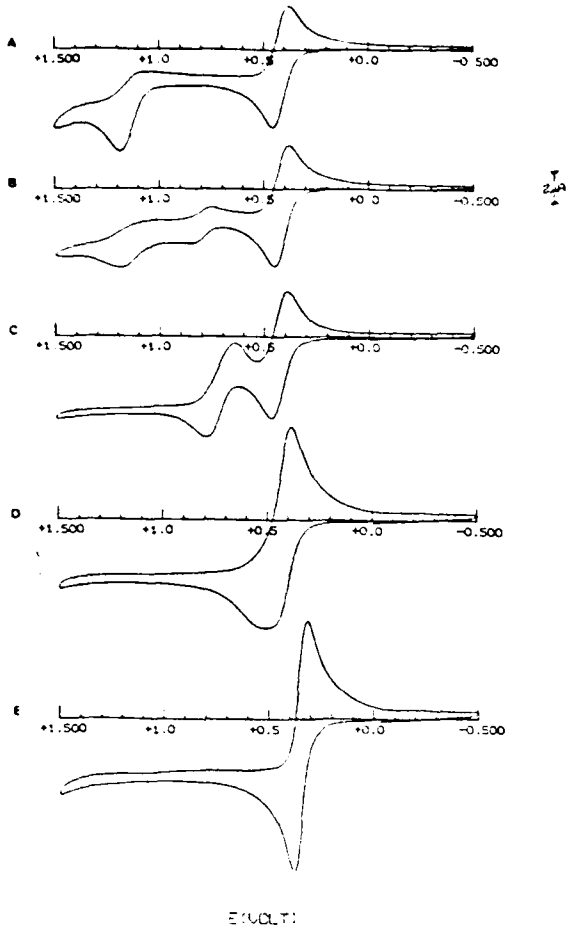

Figure 5. Cyclic voltammetric scans measured for 25 mL of a 0.77 mM solution of $[Ir(\mu\text{-pz})(COD)]_2$ in 1,2-dichloroethane/TBAH at a glassy carbon electrode. All cyclic voltammograms were recorded at 20 mV/s: (A) 0 μL of added CH_3CN/TBAH; (B) 10 μL of added 0.76 M CH_3CN/TBAH; (C) 2 μL of added neat CH_3CN/TBAH; (D) 100 μL of added neat CH_3CN/TBAH; (E) 2100 μL of added neat CH_3CN/TBAH.

is ruled out.

The electrochemical data are compatible with all three schemes, but mechanisms analogous to Scheme I (direct 2e⁻ transfer) have not been verified for other systems. The differentiation of the remaining two schemes requires additional experimental results.

$[Ir(\mu\text{-pz})(COD)]_2$ in Mixed CH_2Cl_2/CH_3CN Solutions. Addition of CH_3CN to CH_2Cl_2 solutions of $[Ir(\mu\text{-pz})(COD)]_2$ causes an interesting series of changes to occur in the CV experiment. We identify three distinct sets of CV behavior as illustrated in Table II.

Case A. The stepwise addition of subequivalent amounts of CH_3CN to a 4.94 mM solution of $[Ir(\mu\text{-pz})(COD)]_2$ in CH_2Cl_2 results in the behavior labeled A in Table II. With each addition of CH_3CN to the solution, $E_{p,a}$ at +1.28 V for the second chemically irreversible oxidation gradually decreases in intensity and a new, quasi-reversible wave grows into the CV with $E_{p,a}$ at +0.849 V at v = 100 mV/s. An analogous change occurs in DCE/TBAH solutions as illustrated in Figure 5A and 5B. This behavior is indicative of strong, reversible complexation of the two-electron oxidized binuclear complex:

$$[Ir(\mu\text{-pz})(COD)]_2^{2+} + p CH_3CN \rightleftharpoons [Ir(\mu\text{-pz})(COD)]_2(CH_3CN)_p^{2+} \quad (19)$$

With the assumption that the peak current, i_p, of the new wave is a measurement of the concentration of complexed, two-electron oxidized binuclear species, the ratio of complexed to uncomplexed two-electron oxidized binuclear can be determined as a function of free $[CH_3CN]$.

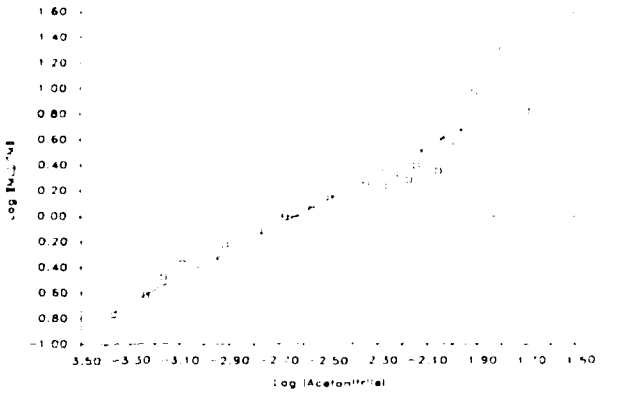

Figure 6. Plot of log {[complexed]/[uncomplexed]} vs. log $[CH_3CN]$ for the sequential addition of 1.9 M CH_3CN/TBAH in CH_2Cl_2/TBAH to a 4.94 mM solution of $[Ir(\mu\text{-pz})(COD)]_2$ in CH_2Cl_2/TBAH. $i_{p,a}$ for the complexed form of $[Ir(\mu\text{-pz})(COD)]_2^{2+}$ was used to compute [complexed]/[uncomplexed] (see Experimental Section). Cyclic voltammetric data were obtained at v = 100 mV/s. Experimental points are presented as squares. The least-squares line has slope = 1.02 and intercept = 2.68.

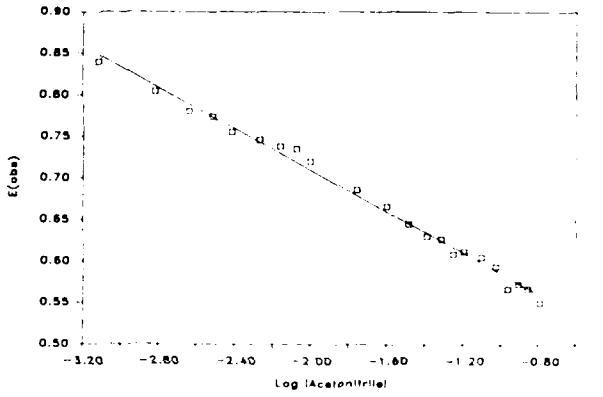

Figure 7. Plot of $E_{p,a}^{2/1}$ vs. log $[CH_3CN]$ for the sequential addition of CH_3CN to a 0.55 mM solution of $[Ir(\mu\text{-pz})(COD)]_2$ in CH_2Cl_2/TBAH. Cyclic voltammetric data were obtained at v = 50 mV/s. Experimental points are represented as squares. The least-squares line has slope = −0.124 V and intercept = +0.462 V.

The plot (eq 1) of log {[complexed]/[uncomplexed]} vs. log $\{[CH_3CN]_{added} - p[complexed]\}$ (Figure 6) gives an excellent straight line with a slope of 1.02 and intercept of 2.68. The slope gives directly the value for p in equilibrium 19. The intercept is then equal to log K_1 = 2.68 (K_1 = 480 M^{-1}). Perhaps most importantly, the quasi-reversible nature of the wave involving the complexed two-electron oxidized form and the determination of K_1 for equilibrium 19 enables an estimate of the $E_{1/2}^{0'}$ of +0.98 V to be made for eq 20.

$$e^- + [Ir(\mu\text{-pz})(COD)]_2^{2+} \rightleftharpoons [Ir(\mu\text{-pz})(COD)]_2^{+} \quad (20)$$

Case B. The results of further sequential additions of CH_3CN aliquots to the 0.77 mM solution of $[Ir(\mu\text{-pz})(COD)]_2$ in 1,2-dichloroethane/TBAH are shown in Figure 5C–5E (v = 20 mV/s). Addition of CH_3CN (Figure 5C: 2 μL of added CH_3CN) causes the wave due to the more positive electrode process to shift to more negative potentials, while the first wave does not shift. Further microliter additions of CH_3CN to the solution cause the more positive wave to shift until it overtakes and merges (Figure 5D: 100 μL of added CH_3CN) with the first wave, to give a single wave (case C) with ΔE_p = 126 mV, and peak currents larger than for either of the two, one-electron waves observed in neat 1,2-dichloroethane/TBAH. Further additions of CH_3CN cause the merged wave to sharpen (Figure 5E: ΔE_p = 75 mV at added CH_3CN = 2100 μL) and continue the shift to more negative potentials.

Analysis of more extensive CV data obtained for a sequential addition experiment with CH_2Cl_2 as the solvent for the $[CH_3CN]$

range where two discrete waves are present was made according to eq 5 (Experimental Section). The plot of $E_{p,a}$ for the second wave vs. log [CH_3CN] is shown in Figure 7. This plot gives a straight line (correlation coefficient = 0.9787, slope = −0.124 V, and intercept = +0.462 V). The slope of this line is indicative of the overall reversible binding of 2.1 ± 0.1 CH_3CN ligands to the *two*-electron oxidized binuclear complex, because the *one*-electron oxidized complex does not bind CH_3CN to an appreciable extent.

$$[Ir(\mu\text{-pz})(COD)]_2^{2+} + 2CH_3CN \rightleftharpoons [Ir(\mu\text{-pz})(COD)(CH_3CN)]_2^{2+} \quad (21)$$

The intercept value gives the total, relative stabilization of the two-electron oxidized form relative to the one-electron oxidized form in 1 M CH_3CN vs. pure CH_2Cl_2/TBAH. The largest contribution to the intercept value is stabilization of $[Ir(\mu\text{-pz})(COD)]_2^{2+}$ via the complexation equilibrium 21. Other contributions to the intercept value include changes in relative solvation energies and, to a lesser extent, small changes (~10 mV) in junction potential. An independent measurement of these effects would be needed to extract log K_1K_2 from the intercept value. When the derived value for $E^{\circ\prime}_1$ of +0.98 V and the intercept value (+0.462 V) are utilized, the net stabilization of $[Ir(\mu\text{-pz})(COD)]_2^{2+}$ in 1 M CH_3CN in CH_2Cl_2/TBAH compared with neat CH_2Cl_2/TBAH is 0.518 V or 11.9 kcal/mol.

Case C. After the free concentration of CH_3CN reaches about 2.0 M, two separate waves are no longer observed. As [CH_3CN] is increased, the combined wave sharpens and continues to shift toward negative potentials. The sequential addition data in the CH_3CN concentration range 2–19 M were not analyzed quantitatively because the shifts are of the same magnitude as the change in junction potential.

Conclusions

In the poorly coordinating solvent CH_2Cl_2, two thermodynamically discrete le processes are observed for the oxidation of $[Ir(\mu\text{-pz})(COD)]_2$. The first wave is quasi-reversible with an $E^{\circ\prime}$ value that is independent of the supporting electrolyte and the presence of water. The second wave is chemically irreversible in dry CH_2Cl_2/TBAH, partially chemically reversible in CH_2Cl_2/TBAP, and chemically reversible in "moist" CH_2Cl_2/TBAH. Bulk electrolyses in CH_2Cl_2 solutions at potentials positive of the first oxidation yield *n* values of two even though *n* for the electrode reaction is one under these conditions. The initially produced radical $[Ir(\mu\text{-pz})(COD)]_2^+$ undergoes a slow reaction with CH_2Cl_2 that yields a two-electron oxidative addition product. Addition of subequivalent amounts of acetonitrile to dichloromethane solutions of $[Ir(\mu\text{-pz})(COD)]_2$ results first in the growth of a new quasi-reversible wave ($E_{p,a}$ at +0.849 V) and in the simultaneous disappearance of the irreversible wave ($E_{p,a}$ = +1.28 V). When sufficient amounts of acetonitrile are added to cause the disappearance of the irreversible wave, the new wave shifts to less positive potentials due to the formation of $[Ir(\mu\text{-pz})(COD)]_2(CH_3CN)_2^{2+}$.

In pure CH_3CN solutions, the concentration of acetonitrile is sufficient to shift the $E^{\circ\prime}_1$ couple to potentials negative of the $E^{\circ\prime}_2$ formal potential. Under these conditions, a single process is observed in the CV, and the bulk electrolysis and electrode reaction *n* values are both 2.0 e⁻/binuclear unit. This result contrasts two different reports in the literature[22,23] from limited CV results that claim *n* = 1 for the oxidation of $[Ir(\mu\text{-pz})(COD)]_2$ in CH_3CN solutions. In view of the sensitivity of the electrochemical response of the $[Ir(\mu\text{-pz})(COD)]_2$ system to medium effects and the presence of small amounts of water, the previous difficulty in determining the mechanistic details of this system is apparent.

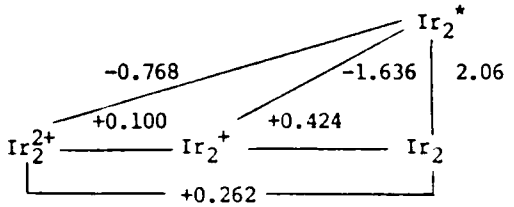

Figure 8. Modified Latimer diagram that illustrates one- and two-electron, ground- and excited-state processes. See ref 24 for details.

Although extrapolation of these results to the photochemical oxidations of $[Ir(\mu\text{-pz})(COD)]_2$ is perhaps speculative, we believe our results may have important implications concerning the thermodynamics of nearly simultaneous two-electron transfers from the lowest excited state of $[Ir(\mu\text{-pz})(COD)]_2$ to suitably designed two-electron acceptors. The electrochemical data allow us to construct a modified Latimer diagram[24] (Figure 8) for $[Ir(\mu\text{-pz})(COD)]_2$ in CH_3CN solutions that include two-electron processes. Because the electron-transfer kinetics of a one-step, two-electron transfer from Ir_2^* may be slow,[5] rapid sequential one-electron transfers during the lifetime of a single solvent cage may prove to be the more kinetically favored pathway for the net two-electron reduction of an acceptor by Ir_2^*. This "kinetic" view would place an additional thermodynamic constraint on net two-electron transfer reactions of Ir_2^*. A negative free energy for the second electron transfer may be required to complete the sequence leading to net, two-electron transfer. As in the case of one-electron excited-state electron transfers, escape from the solvent cage will be required to observe the transient products of the net reaction. The further experimental exposition of these ideas is currently being pursued in our laboratory.

Acknowledgment. We thank John Evans and Harry B. Gray for helpful discussions. Johnson-Matthey Inc. is acknowledged for a generous loan of $IrCl_3 \cdot 3H_2O$.

Supplementary Material Available: Experimental data for the sequential additions of CH_3CN to CH_2Cl_2 solutions of $[Ir(\mu\text{-pz})(COD)]_2$ (Tables 1 and 2) (2 pages). Ordering information is given on any current masthead page.

(22) Marshall, J. L.; Stobart, S. R.; Gray, H. B. *J. Am. Chem. Soc.* **1984**, *106*, 3027.

(23) Bushnell, G. W.; Fjeldsted, D. O. K.; Stobart, S. R.; Zaworotko, M. J.; Knox, S. A. R.; Macpherson, K. A. *Organometallics* **1985**, *4*, 1107.

(24) Ir_2 is used as the abbreviation for $[Ir(\mu\text{-pz})(COD)]_2$. The Latimer diagram is constructed without junction potential corrections. The potential for the 2e⁻ reduction of Ir_2^+ is taken as the E° measured in neat CH_3CN/TBAH solution. E° for the Ir_2^{2+}/Ir_2^+ couple in CH_3CN was estimated from $E^{\circ\prime}_1 - 2E^{\circ\prime}_2 = E^\circ_{1/2}(CH_2Cl_2) = 2(0.262) - (0.424) = 0.100$ V. Excited state potentials were calculated in a manner analogous to ref 22.

(25) Simultaneous two-electron transfers have been the subject of a theoretical investigation, see: Gurnee, E. F.; Magee, J. L. *J. Chem. Phys.* **1957**, *26*, 1237.

"Chemical and Mechanical Properties of Redox Polymer Modified Electrodes. I. A Mechanical/Electrochemical Model", E. F. Bowden, M. F. Dautartas and J. F. Evans, J. Electroanal Chem., in press.

A model is developed to describe the coupling of the mechanical and electrochemical thermodynamics of redox polymer film conversion for systems in which there is a net change in the charge per redox site associated with this redox conversion. The electrostatically forced intrusion of compensating charge, in the form of ions of the supporting electrolyte, into the polymer film is predicted to result in nonNernstian behavior because of the finite void volume within the film and the finite molar volume of the charge compensating ion. The physical consequences of this phenomenon are the forced swelling of the polymer film, a process which in the presence of crosslinks (either covalent or ionic) requires energy input in excess of that needed to carry out the simple electron transfer to/from the redox sites. This energy is consumed in doing work against the elastic framework of the crosslinked polymer matrix, and when couched in terms of an elastic deformation may be considered reversible in the thermodynamic sense. The model developed here treats only the simplest of such mechanical coupling in that reversible, isotropic stress-strain is proposed to account for the nonNernstian thermodynamics of these redox polymer films.

SUMMARY AND CONCLUSIONS

In this paper we have proposed that mechanical work can be coupled to the electrode potential in certain polymer modified electrode systems. Such mechanical work is apparently associated with the elastic expansion and contraction of crosslinked redox polymers due to charge compensating counterion incorporation and expulsion, respectively. We further point out the existence of previously reported chemical systems in which mechanical and chemical energy were shown to be interconvertible. In these systems, mechanical states of crosslinked polymers were altered by changing the chemical composition of bathing solutions. Both pH-induced osmotic pressure changes and redox-induced solubility changes have been elaborated to account for the behavior of these "muscles".

Also, a simple physical model was presented and used to derive an expression for electrode potential. The numerous complications which were absent in the simple model, but which could be present to varying degrees in polymer modified electrode systems, were reviewed. These difficulties in quantifying a very complex situation do not, we feel, detract from the main thrust of the argument. Future experimental effort will be directed towards the independent measurement of both film volume and bulk modulus as functions of potential.

In conclusion, a mechanical free energy model has been proposed as an alternative to various chemical models for explaining superNernstian slopes and broadened linear sweep voltammograms observed for many modified electrodes. More than one of these or other mechanisms can be operative simultaneously, and the measurement of charge and potential alone is clearly insufficient to disentangle them from each other. Consideration of thermodynamic expressions such as equations (10) - (12) strongly indicates the need for new experimental strategies.

"Chemical and Mechanical Properties of Redox Polymer Modified Electrodes. II. Redox Thermodynamics of Plasma Polymerized Vinylferrocene Electrodes", M. F. Dautartas, E. F. Bowden and J. F. Evans, J. Electroanal Chem., in press.

The thermodynamics of thin films (<2000 A) of plasma polymerized vinylferocene (PPVF) deposited on various substrates have been examined in aqueous and nonaqueous electrolytes by controlled potential coulometry. The Nernst plots (E vs log [C_{Fc}+/C_{Fc}o]) of these data give slopes in the range of 120-150 mV/decade. Scanning electron microscopy of thicker films (>4000 A) shows that significant physical damage can occur during electrolysis. These and related observations suggest that the super-Nernstian behavior may be related to stress induced by the forced incorporation of the anion of the supporting electrolyte, as required to maintain electroneutrality within the films. A mechanical/electrochemical model is employed to explain the origin of the excess free energy required to convert ferrocene sites to ferrocenium sites within the PPVF films.

SUMMARY AND CONCLUSIONS

This paper describes the careful electrochemical characterization of thin films of plasma polymerized ferrocene (PPVF) supported on various substrates. These films are found to be continuous even at ellipsometrically determined thicknesses as small as 175 A. High concentrations of electroactive sites (4.5 M in tetra-n-butylammonium perchlorate (TBAP)/acetonitrile) are found. Cyclic voltammetry of PPVF reveals broad, nearly symmetric peaks, the potentials of which are found to be much less dependent on choice of solvent and supporting electrolyte than the corresponding voltmmetry of soluble, hydroxymethylferrocene.

Thermodynamic data for PPVF films were acquired by controlled potential coulometry. The results show superNernstian slopes when plotted as E vs log (C_{Fe}+/C_{Fe}o) which range between 120 and 150 mV per decade. No systematic variation in slope with choice of solvent (water, acetonitrile, methylene chloride) or film thickness was found. The operational formal potential in acetonitrile with TBAP as electrolyte averages 0.424 (±0.008) V vs Ag/AgCl. Scanning electron microscopic examination of very thick films (4500 A), which delaminated during oxidation, reveal tearing which is attributed to excessive tensile stress experienced as electrolyte counterion is forced into these films to charge compensate the pendant ferrocenium ions formed. The SEM observations suggest that the superNernstian behavior which is found in the thermodynamic studies of undamaged films can be explained in terms of a model which involves the reversible coupling of mechanical and electrochemical phenomena. Not only is the involution of this model in the PPVF electochemistry more satisfying than the usual "interaction parameter" interpretations in that it suggests a physical basis for the nonideal thermodynamics, but also fitting of the data to this model returns a value for the mechanical parameter of interest (modulus of elasticity) which is in agreement with values found in similar materials.

"Chemical and Mechanical Properties of Redox Polymer Modified Electrodes. III. Redox Thermodynamics of Linear Polyvinylferrocene Electrodes", E. F. Bowden, M. F. Dautartas and J. F. Evans, J. Electroanal Chem., in press.

The redox thermodynamics of thin films (<2000 A) of linear polyvinylferrocene (LPVF) deposited by spincoating on polished electrode substrates have been studied in tetra-n-butylammonium perchlorate/acetonitrile solutions. Three distinct regions of thermodynamic behavior were revealed through analysis of Nernst plots (E vs log (C_{Fc^+}/C_{Fc^0})) constructed from controlled potential coulometric data. For films which were 0-3% oxidized, superNernstian slopes with values dependent upon electrolyte concentration were attributed to Donnan equilibrium contributions to the electrode potential. This form of LPVF thus appears to function as a simple anion exchanger. Further oxidation (up to ca. 50%) is accompanied by a transition to a second thermodynamic region characterized by subNernstian behavior which is interpreted in terms of an increasing association of ferrocenium/perchlorate ion pairs into dimers or higher order aggregates. Oxidation above 50% results in an abrupt return to superNernstian behavior, for which a mechanical/electrochemical model is proposed. In this third region, the LPVF film is envisioned to be a homogeneous network structure characterized by a high concentration of ionic crosslinks and a capability for sustaining electrochemically induced stress arising from the forced accommodation of neutralizing counterions. The transitions from one thermodynamic region to another are consistent with increasing film ion content as oxidation proceeds. The complexity in thermodynamic redox behavior of LPVF results from the substantial potential-dependent changes in film ion concentration (0 to 6 M) along with a relatively high degree of structural freedom due to the lack of covalent crosslinks.

CONCLUSIONS

It has been found that crosslinking has a profound influence upon the redox thermodynamic behavior of polyvinylferrocene films. LPVF, which lacks covalent crosslinks, exhibits behavior which is more complex than the covalently crosslinked PPVF. The lack of crosslinking leaves LPVF with more degrees of structural freedom to respond to electrochemically induced compositional changes. Thus, LPVF exhibits a subNernstian region in which pendant groups apparently have sufficient mobility to interact strongly with each other to create dimers and perhaps higher-order aggregates. Such behavior is absent in PPVF presumably because the covalent network restricts structural reorganization.

Analysis of Nernst plots constructed from equilibrium charge data leads to the conclusion that at least three distinct electrochemical phenomena are involved in controlling thermodynamic behavior. Each appears to dominate in a different region of fractional oxidation of the ferrocenic site population. LPVF films which are <3% oxidized exhibit electrolyte concentration-dependent superNernstian slopes and are found to behave as anion exchange membranes. Further oxidation (up to ca. 50%) results in subNernstian slopes which reflect the increasing aggregation of ferrocenium sites due to ionic interactions. Oxidation above 50% yields superNernstian slopes, and a mechanical/electrochemical model has been proposed to account

for this behavior.

It is important to note that in the overall description of LPVF thermodynamics the transitions from domination by one physical process in a given region to domination by another in an adjacent region are phenomenologically compatible, each being an extension of the other. That is, in the near-reduced state (Region I) the film behaves as an anion exchanger whose free fixed-site concentration increases with fractional oxidation. However, as ion concentrations increase upon further oxidation, ion pair formation and ion pair association become increasingly favored processes and are proposed to dominate in Region II. Thus the transition in thermodynamic behavior from Region I-to-II follows as a natural consequence of increasing ion concentration as the film is oxidized. As ionic association continues to increase, ionic crosslink density also increases while the degrees of structural freedom correspondingly decrease. At the transition separating Regions II and III, approximately half of the redox sites are ionized, and the high degree of crosslinking which has accumulated to this point apparently affords a polymer structure which is likely to be relatively homogeneous at the microscopic level, having acquired significant ionic crystalline character. Ferrocenium and perchlorate concentrations have reached ca. 3 M at this point and the effective exclusion of free solvent is proposed to coincide with the transition. Alternatively, one may consider the possibility that increasing ion concentrations trigger a phase change at the II-to-III transition in which a microscopically heterogeneous Region II structure composed of ionic and non-ionic domains is replaced by a homogeneous, predominately ionic structure in which the existence of free solvent was not energetically favored. In either view the consequence of film ion concentrations above 3 M is an extensively crosslinked Region III structure. Deviations from Nernstian behavior in these films can be interpreted as arising from the need to elastically expand this structure to accommodate additional counterions. In the context of the overall description presented here, there is a logical progression in the structural description of the polymer as its ion content is increased.

"Chemical and Mechanical Properties of Redox Polymer Modified Electrodes. IV. Structural Reorganization of Nafion Films Loaded with Dimethylaminomethylferrocene", Barbara E. Moriarty and John F. Evans, J. Electroanal Chem., submitted.

Nafion films coated on fluorosilanized glassy carbon electrodes were loaded with protonated dimethylaminomethylferrocene ($HAFC^+$) from aqueous sulfuric acid solvent/supporting electrolyte (SSE) solutions. $HAFc^+$ was retained within the polymer films only when the loading solution contained a large concentration of $HAFc^+$ (14-17 mM), and/or a small concentration of acetonitrile (2-5%). These results suggest that the retention of $HAFc^+$ occurs when the ferrocene species are bound to sulfonate exchange sites which are located in relatively more hydrophobic environments. Evidence for a multiplicity of environments within the Nafion is found, and a square scheme mechanism is proposed to explain these results.

Cyclic voltammetric and chronoamperometric experiments carried out after the loaded film was transferred into a solution containing only SSE imply that the Nafion polymer film undergoes a reorganization, accompanied by loss of the less tightly-bound $HAFc^+$ from hydrophilic regions. The resulting films were then found to be stable for several months in SSE solutions.

The addition of acetonitrile to the SSE causes ferrocene species that were initially electroinactive in the $HAFc^+$-loaded films, to become electrochemically active. These results are interpreted in terms of plasticization of the Nafion polymer by the acetonitrile.

SUMMARY AND CONCLUSIONS

The retention of $HAFc^+$ in Nafion films is achieved only by using either large concentrations of $HAFc^+$, or by including a small concentration of a swelling solvent (e.g. acetonitrile) in the SSE. Evidence for multiple environments within the Nafion is given, and the cyclic voltammetric results are interpeted using a square scheme mechanism.

The polymer film reorganizes after transfer from the loading solution to one containing only solvent/supporting electrolyte. This reorganization is accompanied by a cathodic shift in the apparent formal potential, a decrease in the peak separation and a change in the current transients from potential step experiments. After reorganization, the $HAFc^+$-loaded Nafion film is stable for long periods of time (3 months).

Finally, experiments in which acetonitrile was added to solvent/supporting electrolyte after polymer reorganization indicate the presence of other ferrocene sites which are initially electroinactive. These sites can become electrochemically active when a solvent that swells the polymer is added to the solvent/supporting electrolyte.

These experiments demonstrate that polymer coated electrodes are structurally dynamic systems, and that the structural properties of the polymer can markedly influence the electrochemical performance of the film-coated electrodes.

PUBLICATIONS

1. "Synthesis, Characterization, and Properties of Stable Chromium(III) Aryl Isocyanide Complexes", David A. Bohling and Kent R. Mann, Inorg. Chem., 22, 1561 (1983).

2. "X-Ray Structural Characterization of $[Cr(CNPh)_6][CF_3SO_3]$, $[Cr(CNPh)_6][PF_6]_2$ and $[Cr(CNPh)_6][SbCl_6]_3 \cdot CH_2Cl_2$. Completion of a Unique Series of Complexes in Which the Metal Attains Four Different Oxidation States While Maintaining Identical Ligation", David A. Bohling and Kent R. Mann, Inorg. Chem., 23, 1426 (1984).

3. "Electrochemical Redox Behavior of Hexakis-(aryl isocyanide) Complexes of Molybdenum (0) and Tungsten (0)", David A. Bohling, Kent R. Mann, Starla Enger, Thomas Gennet, Michael J. Weaver and Richard A. Walton, Inorg. Chim. Acta, 97, L51 (1985).

4. "Electrochemistry Studies of $[Ir(u\text{-}pz)(COD)]_2$ in Halocarbon and Acetonitrile Solutions. Solvent Control of Sequential Electron-Transfer Thermodynamics", David C. Boyd, Gary S. Rodman and Kent R. Mann, J. Am. Chem. Soc., 108,1779 (1986).

5. "Chemical and Mechanical Properties of Redox Polymer Modified Electrodes. I. A Mechanical/Electrochemical Model", E. F. Bowden, M. F. Dautartas and J. F. Evans, J. Electroanal Chem., in press.

6. "Chemical and Mechanical Properties of Redox Polymer Modified Electrodes. II. Redox Thermodynamics of Plasma Polymerized Vinylferrocene Electrodes", M. F. Dautartas, E. F. Bowden and J. F. Evans, J. Electroanal Chem., in press.

7. "Chemical and Mechanical Properties of Redox Polymer Modified Electrodes. III. Redox Thermodynamics of Linear Polyvinylferrocene Electrodes", E. F. Bowden, M. F. Dautartas and J. F. Evans, J. Electroanal Chem., in press.

8. "Chemical and Mechanical Properties of Redox Polymer Modified Electrodes. IV. Structural Reorganization of Nafion Films Loaded with Dimethylaminomethylferrocene", Barbara E. Moriarty and John F. Evans, J. Electroanal Chem., submitted.

PERSONNEL SUPPORTED ON THIS GRANT

Year	Name	Degree Rec'd or Expected
1982	David A. Bohling	PhD. 1985
	Thomas P. Gill	
	Barbara E. Moriarty	PhD 1986
	John F. Evans	faculty
	Kent R. Mann	faculty
1983	David A. Bohling	PhD. 1985
	David C. Boyd	PhD. 1986
	Barbara E. Moriarty	PhD 1986
	John G. Newman	MS 1984
	John F. Evans	faculty
	Kent R. Mann	faculty
1984	David A. Bohling	PhD. 1985
	Edmond F. Bowden	post-doctoral
	David C. Boyd	PhD. 1986
	Kevin L. Garber	PhD. 1987
	Barbara E. Moriarty	PhD. 1986
	Matthew M. Rhodes	
	Janet L. Schrenk	PhD. 1985
	John F. Evans	faculty
	Kent R. Mann	faculty
1985	David C. Boyd	PhD. 1986
	Kevin L. Garber	PhD. 1987
	Gary S. Rodman	
	Barbara E. Moriarty	PhD. 1986
	John F. Evans	faculty
	Kent R. Mann	faculty

BIBLIOGRAPHY

1. a) K.R. Mann, G.S. Hammond and H.B. Gray, J. Am. Chem. Soc., 99, 306 (1977); b) K.R. Mann, M. Cimolino, G.L. Geoffroy, G.S. Hammond, A.A. Orio, G. Albertini and H.B. Gray, Inorg. Chim. Acta, 16,97 (1976); c) K.R. Mann, Ph. D. Thesis, California Institute of Technology, Pasadena, CA, 1976.

2. a) M.F. Dautartas and J.F. Evans, J. Electroanal. Chem., 109 (1980) 301; b) M.F. Dautartas; K.R. Mann and J.F. Evans, Ibid., 110 (1980) 379.

END

DTIC

8-86